Texture and Speckle Statistics in Polarimetric SAR Synthesized Images

Gianfranco De Grandi, *Fellow, IEEE*, Jong-Sen Lee, *Fellow, IEEE*, Dale Schuler, *Fellow, IEEE*, and Edmond Nezry

***Abstract*—We investigate in this paper the one-point statistical properties of the backscattered power derived by polarization synthesis of polarimetric synthetic aperture radar (SAR) observations. In particular, we focus our attention on the normalized second moment of intensity and its dependency on the polarization state. For the analysis of this dependency, a novel graphical representation—an extension of the polarization response—is introduced: the polarimetric texture signature. The second moment of backscattered power characterizes statistically the variation of the radar signal due to speckle and the underlying radar cross section. The classical texture product model with a scalar radar reflectivity implies that the normalized second moment of intensity does not depend on the polarization state. However, such dependency is found in experimental observations, a fact that calls for further investigation of the phenomenon. Considering at first speckle statistics for homogeneous areas having no texture, it is demonstrated that correlation among the single-look speckle patterns, which are added on an intensity basis in a multilook operation, is responsible for a weak polarization dependency of the normalized second moment. Concerning the textural properties, a new model is proposed—the mixture model—where it is assumed that polarimetrically diverse scattering mechanisms contribute to the total return from an ensemble of resolution elements. Numerical simulations are used to reconstruct the texture signatures according to the mixture model, starting from simple assumptions related to scattering processes from natural targets. It is found that the polarimetric texture signature can be an interesting discriminator of weak targets against clutter, when only polarimetric diversity and not radiometric diversity plays a role. The effects predicted by the theory are confirmed by experimental analysis of polarimetric data acquired by the Jet Propulsion Laboratory AIRSAR sensor. Finally a classification scheme based on the polarimetric texture signature is proposed.**

***Index Terms*—Polarimetry, synthetic aperture radar (SAR) statistics, speckle, texture.**

I. Introduction

MUCH WORK has been reported in the literature about the statistical characterization of polarimetric synthetic aperture radar (SAR) data when the transmitted and scattered electromagnetic waves are measured in a vector basis corresponding to linearly polarized (H, V) fields [1]–[3]. The basic assumption underlying these studies is a vector multiplicative speckle model with a scalar wide-sense stationary radar reflectivity. The backscattered polarimetric signal is, therefore, a vector random variable containing the elements of the scattering matrix (for a deterministic target) or the elements of the sample covariance matrix (for a random target), but the underlying radar reflectivity is modeled by a scalar random variable. This position implies that the radar cross section statistical distribution is independent from the polarization of the incident and scattered waves (see Section II).

In this paper we try to expand the horizon of this research theme in several directions. First we deal with the statistical properties of the backscattered power when the scattering matrix or the sample covariance matrix are represented in a vector basis which is different from the one used in the measurement process (usually H, V). This transformation is called *polarization synthesis* (see Section III).

The problem is tackled using random variable (RV) transformations. The ensemble of polarimetric measurements (the radar resolution elements in space) is a vector RV, and is characterized statistically by a multivariate distribution function. The polarimetric synthesis operation is tantamount to a linear transformation that maps a vector manifold to another. Then if we model or measure the distribution function in one polarimetric basis we can compute, using the classical RV transformation theory, the distribution function in another polarimetric basis (see Section IV).

In the new polarization basis, we can derive expectations and higher order moments at one point in space (one point statistics), at two points in space (correlation and spectral properties), and higher order statistics (cumulants). We will, however, limit our considerations to the one point statistics.

In particular, we are interested in the second moment of the backscattered power. This statistical quantity is linked from a physical point of view to the variation (in space) of the radar signal due to speckle noise and to the intrinsic modulation of the radar cross section (texture). From the polarimetric point of view, we can consider one more dependency, namely the polarization state of the wave. Indeed this is the major focal point of our investigation. Main questions are thus: 1) when and why can we expect the second moment to change with the polarization state? 2) what is the contribution of speckle? and 3) what is the contribution of texture to the overall phenomenon?

For the analysis of the polarimetric dependency of the second moment, we introduce a new representation that encapsulates in graphical form all the needed information. This representation is the natural extension of the polarization signature (or polarization response) introduced by Van Zyl and Agrawal [4]–[7],

Manuscript received November 8, 2001; revised February 21, 2003.

F. De Grandi is with the European Commission, Joint Research Center, Institute for Environment and Sustainability, TP 440, 21020 Ispra, Varese, Italy (e-mail: frank.de-grandi@jrc.it).

J.-S. Lee and D. L. Schuler are with the Remote Sensing Division, Naval Research Laboratory, Washington, DC 20375-5351 USA (lee@ccs.nrl.navy.mil; dschuler@ccs.nrl.navy.mil).

E. Nezry was with the EC Joint Research Center. He is now with Privateers N.V., 31500 Toulouse, France (e-mail: Edmond.nezry@free.fr).

Digital Object Identifier 10.1109/TGRS.2003.813846

and is called the *polarimetric texture signature* (see Sections V and VI).

It is demonstrated that one mechanism influencing the dependency of the intensity second moment on the wave polarization state is linked to the correlation properties of the single-look speckle patterns used in the multilook image formation (see Section VII). This phenomenon is entirely due to speckle statistics.

The textural properties are investigated next. If the electromagnetic wave sees different geometrical or dielectric properties of the target according to the wave polarization, and if those properties are spatially modulated, then the image texture should also be a function of polarization. Experimental evidence in this direction has been already reported in the literature [9].

Theoretical models of polarimetric radar clutter can be used in conjunction with the RV transformation to characterize the textural component. Models for a constant or a Gamma distributed underlying radar cross section leading to either a complex Gaussian distribution or a multivariate K-distribution of the polarimetric feature vector would, however, not fully account for the polarimetric texture statistics. The models must, therefore, be extended to take into consideration the different radar cross section modulations in the polarimetric channels. One solution is to allow for a vector component of the radar reflectivity in the multiplicative model. We propose here an alternative solution and consider in our ensemble averages resolution elements where the dominating scattering mechanisms are polarimetrically different (e.g., characterized by a different covariance matrix); this gives rise to a mixture model (see Section VIII).

The mixture model can account for both the deviation from wide sense stationarity in selected polarization states (e.g., the presence of weak point targets that backscatter only at selected polarization states), and the combination of polarimetrically different scattering mechanisms within the considered ensemble (e.g., a complex natural target such as a fragmented forest). Moreover the model lends itself nicely to numerical simulation.

Simulation test cases highlight the fact that a polarimetric radar introduces one more degree of information as far as texture in concerned: the difference in textural parameters according to the wave polarization state. We call this phenomenon *polarimetric texture diversity*.

Finally, experimental analysis of airborne polarimetric SAR data (see Section IX) is reported that confirms the theoretical assumptions and demonstrates the usefulness of the polarimetric texture diversity concept.

II. Theoretical Models of Polarimetric Radar Backscatter From Natural Random Targets

We give in this section a synopsis of the models which are relevant for describing the statistics of the backscattered radar signal for distributed natural targets (e.g., forest and terrain clutter) and for stationary texture (either constant or varying at a scale larger than the resolution element). This will lay the foundation for tackling the problem of polarimetric speckle statistics as a transformation of random variables and to introduce the concept of polarimetric diversity, or the asymmetry in the wave scattering mechanism with polarization, which requires an extension of the existing models.

From the mathematical point of view, the basic tool for modeling the statistics of the radar return from an ensemble of correlation volumes is a random walk in n dimensions (two for a scalar radar, and six for a polarimetric radar under the assumption of reciprocity). Indeed since the scattered electric field is a two component phasor, radiation scattered strongly (e.g., with a uniform random distribution of phase) by a large population of objects can be represented as the resultant of a random walk in a plane. The parameters of the random walk can also be identified with physical observables in the scattering phenomenon, and therefore, the bridge between the mathematical tool and the underlying physical world is thus established. Changing the assumptions on the random walk parameters leads to the development of a ladder of models, going from the Gaussian regime and fully developed speckle [22], [25], to the partially developed speckle problems and the class of generalized K-distributions [26], [27], [29]. An alternative view is the so-called multiply stochastic representation [28]. Here the statistics governing the overall phenomenon are seen as a compound form, whereby the mean of one distribution is itself a random variable, governed by a second distribution. For instance, the K-distribution is obtained from an exponential distribution whose mean is itself stochastic and is described by a Gamma distribution. This also leads one to represent the observed variable (or vector) as the product of a textural variable and a fading variable (multiplicative model) [30].

Following this second point of view, a hierarchy of statistical polarimetric models can be defined according to the characteristics of the textural variable. The hierarchy of models is constructed by relaxing progressively the assumption of homogeneity for the textural variable. The first and simplest level consists of a model with a scalar one-dimensional constant texture variable (fully developed speckle regime, constant underlying radar reflectivity, scalar radar). At the last level, the textural variable is a vector and has a different statistical characterization for each component (polarimetric radar and polarimetric texture).

The focus of this paper is on the investigation of statistical aspects that come into play when we consider this last situation. From the physical point of view, this statistical behavior is driven by different scattering mechanisms that come into play and modulate the underlying radar cross section (the textural parameter) according to the polarization state (see Section VIII).

III. Polarization Synthesis

In this section, we give a brief summary of the polarimetric scattering theory related to the representation of plane electromagnetic waves using different polarization bases. This theory lays the groundwork for the calculation of the backscattered power at different transmit and receive polarization states, an operation that is referred to as *polarization synthesis*. Many other research topics in radar polarimetry, such as scattering component decompositions [10], [11], speckle filtering [12]–[14], and classification based on optimum polarization states [15]–[17], rely on this mathematical framework. This section contains formulas, conventions, and terminology that will be used in the rest of the paper.

The theory of polarization synthesis has been extensively presented in the literature [7], [8], [18], [19]. We give here a derivation that relies on the theory of linear vector spaces. In the following, the backscattering alignment convention (BSA) is adopted [18].

A plane electromagnetic wave in any pure state of polarization (elliptical or linear) can be described as the sum of two phasors corresponding to linearly polarized fields oriented along two orthogonal directions in space, e.g., horizontal and vertical. We can, therefore, represent a plane wave in a general state of polarization as a member of a vector space C_2 of pairs of complex numbers $[Le^{j\phi_1}, Me^{j\phi_2}]$. Since the absolute phase is not relevant, the two phasors can be expressed in terms of their complex ratio $\rho = (L/M)e^{j(\phi_1-\phi_2)}$ as [1, ρ]. The complex ratio ρ can also be expressed as a function of the orientation and ellipticity angles [19] as

$$\rho = \frac{\cos(2\tau)\sin(2\psi) + j\sin(2\tau)}{1+\cos(2\tau)\cos(2\psi)}. \tag{1}$$

A definition of the orientation and ellipticity angles with respect to the polarization ellipse (loci of the electric field vector in the plane of the travelling wave) is given, for instance, in [18]. Throughout this paper, we will use the notation

$$\begin{aligned} \psi(0 \to \pi) &= \text{orientation angle} \\ \chi\left(-\frac{\pi}{4} \to \frac{\pi}{4}\right) &= \text{ellipticity angle}. \end{aligned} \tag{2}$$

The angle ψ is measured with respect to the horizontal axis.

An orthonormal basis corresponding to a general state of polarization ρ and with respect to the inner product defined in C_2 is

$$\left[\frac{1}{\sqrt{1+\rho\rho^*}}, \frac{\rho}{\sqrt{1+\rho\rho^*}}\right]\left[\frac{-\rho^*}{\sqrt{1+\rho\rho^*}}, \frac{1}{\sqrt{1+\rho\rho^*}}\right]. \tag{3}$$

The unitary transformation $\mathbf{A}\,(\mathbf{A}^+\mathbf{A} = \mathbf{I})$ that maps a vector from the linearly polarized (H, V) basis to the basis corresponding to polarization state ρ is

$$\mathbf{A} = \frac{1}{\sqrt{1+\rho\rho^*}}\begin{bmatrix} 1 & \rho^* \\ -\rho & 1 \end{bmatrix}. \tag{4}$$

The scattering properties of a deterministic target are completely characterized by the complex scattering matrix, which maps the transmitted and received fields: $\mathbf{E_R} = \mathbf{S}\mathbf{E_T}$.

Therefore, $\mathbf{A}\mathbf{E_R} = \mathbf{S'}\mathbf{A}\mathbf{E_T}$ and the scattering matrix in the new basis is given by

$$\mathbf{S}' = \mathbf{A}\mathbf{S}\mathbf{A}^{-1}. \tag{5}$$

The scattering matrix can also be represented for a reciprocal system by a three-component feature vector $\mathbf{x} = (S_{\mathrm{HH}}, \sqrt{2}S_{\mathrm{HV}}, S_{\mathrm{VV}})$. By similar arguments the unitary transformation that maps this vector is

$$\mathbf{T}(\rho) = \frac{1}{1+\rho\rho^*}\begin{bmatrix} 1 & \sqrt{2}\rho & \rho^2 \\ -\sqrt{2}\rho^* & 1-\rho\rho^* & \sqrt{2}\rho \\ \rho^{*2} & -\sqrt{2}\rho^* & 1 \end{bmatrix}. \tag{6}$$

In SAR multilook data, a resolution element is obtained from a number of single-look resolution elements in the azimuth sample space. Multilooking for polarimetric data is described sometimes as an incoherent average of the scattering matrices associated with the single-look elements. We prefer the following statistical point of view. Single-look samples can be considered as separate scalar random variables $s_1 \cdots s_n$, and the multilook operation forms a vector random variable $\mathbf{s} = (s_1, \ldots, s_n)$, which is characterized by its covariance matrix $\mathbf{C_S} = E[\mathbf{s}\mathbf{s}^+]$, where $E[\cdot]$ is the expected value operator; $\mathbf{s}^+$ is the conjugate transpose of $\mathbf{s}$ and the outer product gives an $n \times n$ matrix. There can be no equivalent scattering matrix for the multilook element, because physically it is not a summation of fields, and because statistically we need to represent the second-order properties given by the product $\mathbf{s}\mathbf{s}^+$. Also note the subscript S in $\mathbf{C_S}$, which stands for "sample" and, thus, clearly distinguishes the covariance matrix that characterizes the single resolution element from the ensemble covariance matrix $\mathbf{C_E}$ that characterizes a field of resolution elements (ensemble average of many $\mathbf{C_S}$).

The multilook dataset, therefore, is a collection of sample covariance matrices, which characterize completely from the statistical point of view an underlying ensemble of scalar random variables (the single-look elements), and not the resultant of any operation involving physical quantities, such as electric fields or associated powers.

The sample covariance matrix is transformed under a change of polarization basis as [19]

$$\mathbf{C_S}(\rho) = \mathbf{T}(\rho)\,\mathbf{C_S}\mathbf{T}^+(\rho). \tag{7}$$

The fact that the scattering matrix and the covariance matrix are mapped into a new polarization basis by a linear transformation is important for further analysis of the transformation of the probability distribution function.

IV. Probability Distribution Function Transformation Induced by Polarization Synthesis

The polarization synthesis operation can be considered as a linear operator (6) on the feature vector $\mathbf{x} = \left(S_{\mathrm{HH}}, \sqrt{2}S_{\mathrm{HV}}, S_{\mathrm{VV}}\right)$ for single-look data. We are interested in investigating how the statistical properties of $\mathbf{x}$ (considered as a vector RV), are affected by a change of the orthonormal basis used to represent the vector. Given a vector RV $\mathbf{x}$ in the (H, V) basis, in a different polarization basis, say (A, B) this vector RV will have a new distribution

$$\mathrm{pdf}_{(\mathrm{A,B})} = f\left(\mathrm{pdf}_{(\mathrm{H,V})}\right). \tag{8}$$

From $\mathrm{pdf}_{(\mathrm{A,B})}$, we will be able to make inferences on the statistical properties of the polarimetric vector in the new basis. We will consider next two cases for a scalar texture variable and single-look uncorrelated complex fields (see models in Section II): complex normal distribution, and multivariate K-distribution.

From the physical point of view, the first case can be modeled as a random walk in two dimensions with a large number $N \to \infty$ of independent phasors (elementary scatterers) and a

uniform distribution of phases (strong scattering). In the second case, the number N of scatterers fluctuates according to a binomial distribution. A single-channel instrument will involve the complex addition of one such random walk. A polarimetric instrument will involve M random walks, one for each channel. Under the hypothesis that the same elementary scatterers are seen by the M channels, so that the random walks will have the same number of steps for each channel, the form of the statistical distribution of the returned power—and related properties—will not depend on the polarization state. When waves in different polarization states see different scatterers the total contribution of the elementary scatterers will not be governed any more by the same random walk, and an extension of the model is required to describe the dependency of the statistical properties from the polarization state. This situation is considered in Section VIII.

A. Complex Normal Distribution

In this case, the probability density function (pdf) of the vector $\mathbf{x}$ in the (H, V) basis is a multivariate complex normal distribution $C\aleph(0, \mathbf{C})$ with zero-mean and complex covariance matrix C. We recall the property that a normal distribution remains normal under a linear transformation of the random vector [33]. Thus

$$\mathbf{x} \in C\aleph(0, \mathbf{C}) \text{ then } \mathbf{y} = \mathbf{T}\mathbf{x} \in C\aleph(0, \mathbf{T}\mathbf{C}\mathbf{T}^{+}). \tag{9}$$

In our study, we are interested in the synthesized intensity $I_{(\mathrm{A,B})}$ in a certain polarization basis (A, B) and the normalized second-order moment of intensity. These can be computed as follows.

Due to the properties of complex Gaussian random vectors, the marginal distribution of any component of $\mathbf{x}$ (e.g., S_{HH}) will be again complex Gaussian with covariance matrix

$$\mathbf{C} = \begin{bmatrix} \sigma_I^2 & 0 \\ 0 & \sigma_Q^2 \end{bmatrix} \tag{10}$$

where $\sigma_I^2 = \sigma_Q^2$ are the variances of the real and imaginary parts.

The marginal distributions of the intensities, therefore, obey a negative exponential law; the nth moment is given by $E[I^n] = n!\,(E[I])^n$.

By applying the linear transformation (6), the feature vector $\mathbf{y}$ in the new basis will have covariance matrix $\mathbf{C}' = \mathbf{T}\mathbf{C}\mathbf{T}^{+}$, the mean intensity and second moment will change, but since $E\left[I_{\mathrm{A,B}}^2\right] = 2E\left[I_{\mathrm{A,B}}\right]^2$ the normalized second moment will not change.

B. Zero-Mean Multivariate K-Distribution

We want to compute the distribution of the vector $\mathbf{y} = \mathbf{T}\mathbf{z}$ where $\mathbf{z}$ is a multivariate K-distributed zero-mean real vector holding the in-phase and quadrature phase components of the polarimetric vector $\mathbf{x}$ [29], and $\mathbf{T}$ is a linear transformation. We recall at first that the characteristic function of $\mathbf{y}$ is given [33] by

$$\Phi_y(\mathbf{v}) = E\left[\exp\left(j\mathbf{v}^{\mathbf{T}}\mathbf{y}\right)\right] = \Phi_z\left(\mathbf{T}^{\mathbf{T}}\mathbf{v}\right) \tag{11}$$

where Φ_z is the characteristic function of the vector RV $\mathbf{z}$, and $\mathbf{v}$ (the independent variable of the characteristic function Φ_y) is a vector with same dimension as $\mathbf{y}$.

The characteristic function of $\mathbf{z}$ when it is zero-mean K-distributed with covariance matrix $\mathbf{C}$ as given in [29] is

$$\Phi_z(\mathbf{k}) = \left[1 + \frac{1}{2\alpha}\mathbf{k}^{\mathbf{T}}\mathbf{C}\mathbf{k}\right]^{-\alpha}. \tag{12}$$

Since $\mathbf{k}^T = \left(\mathbf{T}^T\mathbf{v}\right)^T = \mathbf{v}^T\mathbf{T}$ then

$$\Phi_y(\mathbf{v}) = \Phi_z\left(\mathbf{T}^T\mathbf{v}\right) = \left[1 + \frac{1}{2\alpha}\mathbf{v}^T\left(\mathbf{T}\mathbf{C}\mathbf{T}^T\right)\mathbf{v}\right]^{-\alpha}. \tag{13}$$

Therefore, the transformed vector $\mathbf{y}$ will be again zero-mean K-distributed but with covariance matrix $\mathbf{C}' = \mathbf{T}\mathbf{C}\mathbf{T}^T$.

The second-order normalized moment of the intensity for each component of the polarimetric feature vector $\mathbf{z}$ is given by [26]

$$\overline{m}_2 = 2\left(1 + \frac{1}{\alpha}\right) \tag{14}$$

where, for instance, for the HH component

$$\overline{m}_2 = \frac{E\left[\left(\mathrm{hh}\cdot\mathrm{hh}^*\right)^2\right]}{E\left[\mathrm{hh}\cdot\mathrm{hh}^*\right]^2}.$$

It is, therefore, independent from the covariance matrix and the polarization basis and dependent only on the bunching parameter α. Ways of estimating this parameter are suggested, for instance, in [34].

V. Polarimetric Texture Signature

From the unitary transformation (6), the expected value of the backscattered power in the co-polarized and cross-polarized configurations can be computed as a function of the transmitted and received wave polarization state

$$E[I] = f(\psi_T, \chi_T, \psi_R, \chi_R) \tag{15}$$

where $\psi_R = \psi_T$ $\chi_R = \chi_T$ in the co-polarized configuration and $\psi_R = \pi/2 + \psi_T$ $\chi_R = -\chi_T$ in the cross-polarized configuration.

The expected value of intensity is, therefore, a function of two variables and can be represented graphically as a three-dimensional (3-D) surface. Such a representation was proposed by Van Zyl [4] and is known as the *polarization signature* or the *polarization response*. The representation condenses in graphical form a number of properties related to the polarimetric response of the scatterer.

We propose here to extend such a formalism to higher order moments of the one point statistics. In particular, since we are dealing with texture and speckle statistics in polarimetric imagery, the normalized second-order moment appears to be of interest, because it gives a measure of the speckle strength and of the textural properties.

Accordingly we consider

$$\overline{m}_2 = \frac{E\left[I^2\right]}{E[I]^2} = f(\psi_T, \chi_T, \psi_R, \chi_R). \tag{16}$$

Again we have a function of two variables in the co-polarized and cross-polarized case and a graphical representation as

a 3-D surface will give us a synoptic picture of the textural properties as a function of polarization. In analogy with the polarization signature, we call this representation the *polarimetric texture signature*. The usefulness of the signature formalism for the analysis of the statistical properties of the polarimetric signal will be demonstrated in Sections VIII and IX.

Note that the normalized second-order moment is also linked to the standard deviation normalized by the mean, a quantity that is used as a measure of texture (sometimes called contrast)

$$\frac{E\left[I^2\right]-E\left[I\right]^2}{E\left[I\right]^2}=\overline{m}_2-1. \tag{17}$$

Expected values in (17) are estimated by sample means; bias and variance for the estimators can be found in [20].

The same mechanism could be in principle extended to the two point statistics, e.g., to the intensity autocorrelation function.

Texture signatures corresponding to the two polarization state configurations—co-polarized and cross-polarized—bear different information about the underlying scattering mechanisms. Insight into the issue can be gained considering the power synthesis operation as a linear combination of the covariance matrix terms

$$\begin{aligned} I\left(\psi_T,\psi_R,\chi_T,\chi_R\right)=&w_1\cdot E\left[\mathrm{hh}\cdot\mathrm{hh}^*\right]+w_2\cdot E\left[\mathrm{hv}\cdot\mathrm{hv}^*\right]\\ &+w_3\cdot E\left[\mathrm{vv}\cdot\mathrm{vv}^*\right]+w_4\cdot E\left[\mathrm{hh}\cdot\mathrm{vv}^*\right] \end{aligned} \tag{18}$$

where for simplicity we have assumed $E\left[\mathrm{hh}\cdot\mathrm{hv}^*\right]=E\left[\mathrm{vv}\cdot\mathrm{vh}^*\right]=0$.

Computing the weights $w_i=f\left(\psi_T,\chi_T,\psi_R,\chi_R\right)$ for the co-polarized and cross-polarized case allows us to make the following observations.

In the co-polarized case, the co-polarized power terms $E\left[\mathrm{hh}\cdot\mathrm{hh}^*\right]$ $E\left[\mathrm{vv}\cdot\mathrm{vv}^*\right]$ and the cross-polarized power term $E\left[\mathrm{hv}\cdot\mathrm{hv}^*\right]$ are always mixed together in different proportions while the orientation angle spans the range 0° to 180° for a certain value of the ellipticity angle. On the contrary for the cross-polarized case the co-polarized powers are added in phase, and the cross-polarized power is out of phase by 45°. As a consequence there are polarizations states (0°, 45°, and 90°) where the contributions from the co-polarized powers and cross-polarized power are completely decoupled.

As explained in the following sections, polarimetric texture can be seen as a consequence of an imbalance in the statistical properties of the co-polarized channels and cross-polarized channels. A case in point is the mixture of dihedral type point scatterers embedded in clutter. The polarimetric texture must be computed in the cross-polarized configuration to be sensitive to this type of imbalance. For this reason, in the following only the cross-polarized signature will be dealt with.

For the sake of clarity and conciseness, we adopt the following terminology:

- m1copol: power signature in the co-polarized configuration;
- m1xpol: power signature in the cross-polarized configuration;
- m2xpol: second-order normalized moment signature in the cross-polarized configuration.

A fast numerical computation of the polarimetric texture signature (16) over an ensemble of resolution elements can be implemented in the case of the Stokes scattering operator representation [18] by computing spatial averages of suitable functions of the Stokes scattering operators before the synthesis operation (see (21)–(23) below). A derivation of the algorithm is given next.

Power synthesis for one resolution element is given by

$$\begin{aligned} I_i\left(\psi,\chi\right)=&\mathbf{g}_R^T\left(\psi,\chi\right)\left(\mathbf{M}^i\cdot\mathbf{g}_T\left(\psi,\chi\right)\right)\\ =&\sum_k\sum_m M_{km}^i\left(\psi,\chi\right)S_{km}\left(\psi,\chi\right) \end{aligned} \tag{19}$$

where I_i is the backscattered power; $\mathbf{M}^i$ is the Stokes scattering operator of the resolution element i; $\mathbf{g}_R^T$ is the transpose of the received wave Stokes vector; $\mathbf{g}_T$ is the transmitted wave Stokes vector; and $\mathbf{S}$ is a matrix equal to the outer product $\mathbf{g}_R\mathbf{g}_T^T$.

Define an arrangement by rows of the matrices $\mathbf{M}^i$ and $\mathbf{S}$ into vectors

$$Mv^i_{k=(j-1)L+m}=M^i_{jm}\quad Sv_{k=(j-1)L+m}=S_{jm} \tag{20}$$

where L is the dimension of the matrix representing the Stokes operator.

The sample averages in (16) are then computed as

$$\langle I\rangle=\frac{1}{N}\sum_k\sum_l Mv_l^kSv_l=\sum_l\langle Mv\rangle_lSv_l \tag{21}$$

$$\begin{aligned} I_k^2=&\left(\sum_l Mv_l^kSv_l\right)^2=\sum_l\left(Mv_l^k\right)^2Sv_l^2\\ &+\sum_{j\neq i}Mv_i^kMv_j^kSv_iSv_j \end{aligned} \tag{22}$$

$$\begin{aligned} \left\langle I_k^2\right\rangle=&\frac{1}{N}\sum_l\left(\sum_k\left(Mv_l^k\right)^2\right)Sv_l^2\\ &+\frac{1}{N}\sum_{j\neq i}Sv_iSv_j\sum_k Mv_i^kMv_j^k \end{aligned} \tag{23}$$

where N is the number of resolution elements in the sample averages.

Summations involving the quantities Mv_i^k can be precomputed using fast vector operations on the area of interest. The synthesis operation is then performed as a second step using the averaged quantities.

Procedures for the computation of the texture signature have been implemented using the IDL language.[1]

VI. Texture Signature Decomposition

In this section, we present a technique for decomposing the polarimetric texture signature into a basis constituted by functions that depend only on the transmit and receive polarization state. This technique is useful for interpreting the scattering mechanisms that underpin the graphical representation of the texture signature.

An alternative formulation [21] of the polarimetric synthesis equation decomposes the backscattered power into terms comprising the covariance matrix elements and functions which are

[1]IDL is data visualization and analysis software By Research Systems Inc. (RSI)

dependent only on the polarization basis. For the cross-polarized case and the ensemble covariance matrix $\mathbf{C_E}$, the result is

$$\begin{aligned}P(\mathbf{C_E},\psi,\chi) &= |X_1|^2 C_{E\text{hhhh}} + |X_2|^2 C_{E\text{hvhv}} + |X_3|^2 C_{E\text{vvvv}} \\ &\quad + 2\text{Re}\,[X_1X_3]\,\text{Re}\,[C_{E\text{hhvv}}] - 2\text{Im}\,[X_1X_3]\,\text{Im}\,[C_{E\text{hhvv}}] \\ &\quad + 2\text{Re}\,[X_1X_2]\,\text{Re}\,[C_{E\text{hhhv}}] - 2\text{Im}\,[X_1X_2]\,\text{Im}\,[C_{E\text{hhhv}}] \\ &\quad + 2\text{Re}\,[X_2X_3]\,\text{Re}\,[C_{E\text{vvvh}}] - 2\text{Im}\,[X_2X_3]\,\text{Im}\,[C_{E\text{vvvh}}]\end{aligned} \tag{24}$$

where

$$\begin{aligned}X_1 &\equiv \left(-\frac{1}{2}\right)(\sin 2\psi \cos 2\chi + j \sin 2\chi) \\ X_2 &\equiv -\cos 2\psi \cos 2\chi \\ X_3 &\equiv \frac{1}{2}(\sin 2\psi \cos 2\chi - j \sin 2\chi).\end{aligned} \tag{25}$$

The functions X_1, X_2, and X_3 when plotted versus ψ and χ give a set of characteristic elementary shapes, or "eigenshapes," that can be visually used to decompose the overall signature into the dominant contributions according to the weight given by the elements of the covariance matrix $\mathbf{C_E}$.

A similar decomposition can be worked out for the m2xpol signature. Starting from (16) and (24), we can write the m2xpol as

$$\frac{E\left[I^2\right]}{E\left[I\right]^2} = \frac{\sum_i \xi_i^2 \langle \sigma_i^2 \rangle + \sum_k \sum_i \xi_k \xi_i \langle \sigma_k \sigma_i \rangle}{\sum_i \xi_i^2 \langle \sigma_i \rangle^2 + \sum_k \sum_i \xi_k \xi_i \langle \sigma_k \rangle \langle \sigma_i \rangle} \tag{26}$$

where ξ_i are the factors in (24) containing the functions X_i (e.g., $\xi_1 = |X_1|^2$); σ_i are the factors in (24) corresponding to elements of the sample covariance matrices; and $\langle \cdot \rangle$ are ensemble averages.

This expression can be rewritten as

$$\begin{aligned}\frac{E\left[I^2\right]}{E\left[I\right]^2} &= \frac{\sum_i \xi_i^2 A_i \langle \sigma_i \rangle^2 + \sum_k \sum_i \xi_k \xi_i B_{ki} \langle \sigma_k \rangle \langle \sigma_i \rangle}{\sum_i \xi_i^2 \langle \sigma_i \rangle^2 + \sum_k \sum_i \xi_k \xi_i \langle \sigma_k \rangle \langle \sigma_i \rangle} \\ A_i &= \frac{\langle \sigma_i^2 \rangle}{\langle \sigma_i \rangle^2}, \quad B_{ki} = \frac{\langle \sigma_k \sigma_i \rangle}{\langle \sigma_k \rangle \langle \sigma_i \rangle}\end{aligned} \tag{27}$$

where A_i are normalized second-order moments of the RVs σ_i and B_{ki} are normalized cross-correlations of the same RVs.

What this equation tells us is that variations of the signature in the (ψ, χ) space are due to an imbalance in the coefficients A_i, B_{ki}; each coefficient is associated with a function ξ_i, which has a fixed geometrical representation in the (ψ, χ) space. Therefore, it will provoke a distortion in the flatness of the signature which is related to this elementary shape. Moreover the weight of this distortion is proportional to the squares and cross products of ensemble covariance matrix element $\langle \sigma_i \rangle$. The number of terms, and hence of eigenshapes, involved in (27) is by far too high to be useful in practice; however, it is possible to consider a simplified case where reciprocity and reflection symmetry of the scatterer are assumed, and only the dependency on orientation angle is considered (linear polarization). Examples of the texture signature decomposition are reported in Section IX.

VII. Polarimetric Texture Modulation Due to the Sum of Correlated Speckle Patterns

We consider, in this section, speckle statistics for homogeneous areas having no texture and investigate a first mechanism that influences the dependency of the intensity second moment on the wave polarization state. It is demonstrated that this mechanism is linked to the correlation properties of the single-look speckle patterns used in the multilook image formation.

The multilook operation can be performed in the space domain, summing on an intensity basis single-look data. This was actually the case for the Jet Propulsion Laboratory (JPL) airborne SAR (AIRSAR) data processed at the time of the 1989 Maestro campaign. For polarimetric data, the sum is performed on the Stokes scattering operators, from which the returned power can be synthesized. The sum and synthesis operators can be commuted

$$P = \sum_i \mathbf{g_R^+ M_i g_T} = \mathbf{g_R^+} \left(\sum_i \mathbf{M_i} \right) \mathbf{g_T} \tag{28}$$

where $\mathbf{M_i}$ is the Stokes scattering operator, and $\mathbf{g_R g_T}$ are the received and transmitted Stokes vectors.

Therefore, the power corresponding to a certain polarization state ρ in the multilook operation is equivalent to the sum of single-look intensities, which are synthesized in the same polarization state

$$P(\rho) = \sum_{i=1}^{\text{nlooks}} I_i(\rho). \tag{29}$$

We want to demonstrate that if the single-look complex polarimetric data within the multilook cell are circular Gaussian and correlated, then the probability distribution function of the resulting intensity will be a function of the polarization state. In particular, we will derive numerical estimates of the variation of the normalized second moment as a function of the polarization state.

The case of addition on an intensity basis of correlated speckle patterns is discussed in [22]. To set the ground, we summarize here the results in the case of two speckle patterns. Suppose the two complex Gaussian fields S_1 and S_2 are correlated with second-order (or correlation) matrix

$$C_{(\text{H,V})} = \begin{bmatrix} E\left[S_1 S_1^*\right] & E\left[S_1 S_2^*\right] \\ E\left[S_2 S_1^*\right] & E\left[S_2 S_2^*\right] \end{bmatrix}. \tag{30}$$

The pdf of the sum of the intensities ($I = I_1 + I_2$) can be computed by projecting the vector $\mathbf{a} = [S_1, S_2]^T$ into a basis where the matrix $\mathbf{C}$ is diagonalized. The problem is then conducted to the classical case of the sum of uncorrelated exponentially distributed intensities.

If λ_1, λ_2 are the nondegenerate eigenvalues of the Hermitian correlation matrix $\mathbf{C}_{(\text{H,V})}$ then the pdf of the resulting intensity is

$$\text{pdf}(I) = \left(\frac{e^{-I/\lambda_1}}{\lambda_1 - \lambda_2} - \frac{e^{-I/\lambda_2}}{\lambda_1 - \lambda_2} \right). \tag{31}$$

The second moment is

$$E\left[I^2\right] = 2\left(\frac{\lambda_1^3}{\lambda_1 - \lambda_2} - \frac{\lambda_2^3}{\lambda_1 - \lambda_2} \right). \tag{32}$$

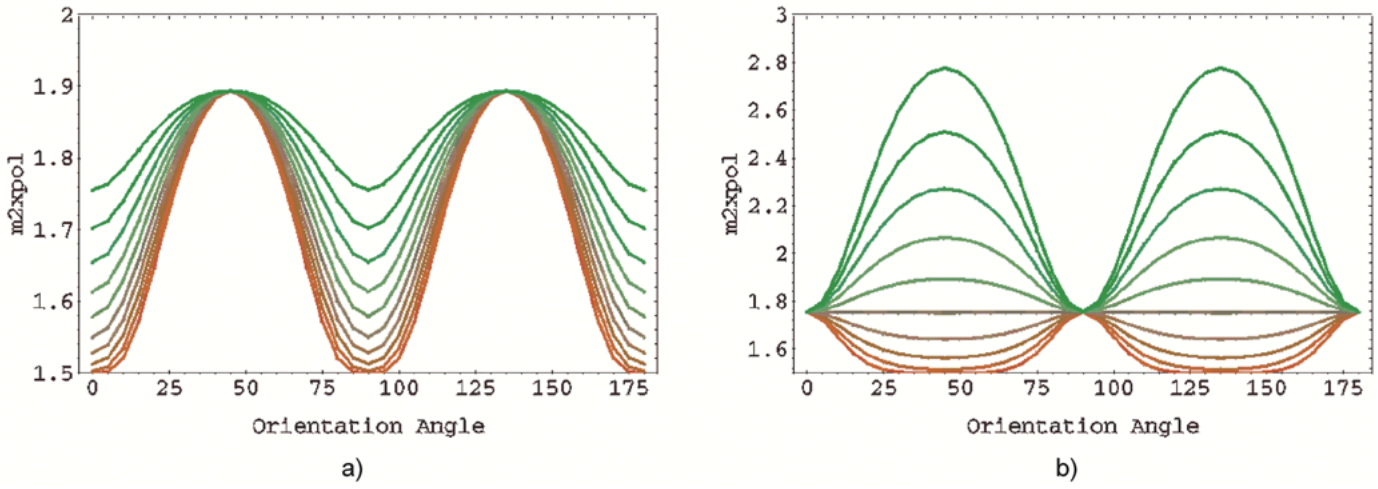

Fig. 1. Theoretical cross-polarized polarimetric texture signature (cross section for linear polarization) in the case of intensity addition of two correlated complex Gaussian speckle patterns. In frame (a), the complex correlation coefficients between speckle patterns are $|\langle {}_1S_{\rm HH} \cdot {}_2S^*_{\rm HH}\rangle| = 0.5$, $|\langle {}_1S_{\rm VV} \cdot {}_2S^*_{\rm VV}\rangle| = 0.5$, and $|\langle {}_1S_{\rm HV} \cdot {}_2S^*_{\rm HV}\rangle|$ varies from 0.0 to 0.09 (family of curves from red to green). The signature shows two distinctive maxima at $\psi = 45°$ and $\psi = 135°$. This characteristic feature is also observed in experimental SAR data (see Section IX). For orientation angles $\psi = 0°$ and $\psi = 90°$ (H-V) basis and for $|\langle {}_1S_{\rm HV} \cdot {}_2S^*_{\rm HV}\rangle| = 0.0$ m2xpol tends to the nominal value of 1.5 for two looks fully developed speckle regime. The sensitivity of the texture signature to the cross-polarized speckle patterns correlation should be also noticed. In frame (b), the sensitivity of the polarimetric texture signature with respect to the correlation between the co-polarized speckle patterns is demonstrated. As the correlation decreases (green to red lines in the graphic), the signature maxima at $\psi = 45°$ and $\psi = 135°$ decrease and become minima. For low correlation values, the maxima are shifted at $\psi = 0°$ and $\psi = 90°$.

Suppose now to transform the single-look speckle patterns into a new polarization basis, say (A, B), using the linear transformation $\mathbf{T}(\rho)$ in (6) and to consider the correlation matrix $\mathbf{C}_{(\rm A,B)}$ in the new basis for the cross-polarized channel

$$\begin{aligned} {}_1S_{\rm AB} &= \sum_k T_{2k}\, {}_1S_k \\ {}_2S_{\rm AB} &= \sum_k T_{2k}\, {}_2S_k \end{aligned} \tag{33}$$

$$\begin{aligned} E\left[{}_1S_{\rm AB} \cdot {}_2S^*_{\rm AB}\right] = &\left(2\rho^{*2} E\left[{}_1S_{\rm HH} \cdot {}_2S^*_{\rm HH}\right]\right. \\ &+ \left(1-\rho^2\rho^{*2}\right) E\left[{}_1S_{\rm HV} \cdot {}_2S^*_{\rm HV}\right] \\ &+ 2\rho^2 E\left[{}_1S_{\rm VV} \cdot {}_2S^*_{\rm VV}\right] \\ &\left.-4\rho\rho^* E\left[{}_1S_{\rm HH} \cdot {}_2S^*_{\rm VV}\right]\right) \cdot \frac{1}{\left(1-\rho\rho^*\right)^2} \end{aligned} \tag{34}$$

$$\begin{aligned} E\left[{}_1S_{\rm AB} \cdot {}_1S^*_{\rm AB}\right] = &\left(2\rho^{*2} E\left[\left|{}_1S_{\rm HH}\right|^2\right]\right. \\ &+ \left(1-\rho^2\rho^{*2}\right) E\left[\left|{}_1S_{\rm HV}\right|^2\right] \\ &+ 2\rho^2 E\left[\left|{}_1S_{\rm VV}\right|^2\right] \\ &\left.-4\rho\rho^* E\left[{}_1S_{\rm HH} \cdot {}_1S^*_{\rm VV}\right]\right) \cdot \frac{1}{\left(1-\rho\rho^*\right)^2} \end{aligned} \tag{35}$$

where we have assumed that $E\left[{}_1S_{\rm HH} \cdot {}_2S^*_{\rm HV}\right] = 0$ and $E\left[{}_1S_{\rm VV} \cdot {}_2S^*_{VH}\right] = 0$. A similar expression holds for $E\left[{}_2S_{\rm AB} \cdot {}_2S^*_{\rm AB}\right]$.

The elements of the correlation matrix $\mathbf{C}_{(\rm A,B)}$ in the new basis are, therefore, a function of the polarization state ρ, of the correlation between the speckle patterns in the original basis (correlation matrix $\mathbf{C}_{(\rm H,V)}$) and the covariance matrix $E\left[S_{ij}S^*_{ij}\right]$ of each speckle pattern vector ${}_1S = ({}_1S_{\rm HH},\ {}_1S_{\rm HV},\ {}_1S_{\rm VV})$ and ${}_2S = ({}_2S_{\rm HH},\ {}_2S_{\rm HV},\ {}_2S_{\rm VV})$ in the original basis.

Substituting the eigenvalues of the correlation matrix $\mathbf{C}_{(\rm A,B)}$ into (32) allows us finally to compute the second moment of the multilook cross-polarized intensity variable as a function of the polarization state ρ.

In summary, the linear transformation into a new polarization basis affects the correlation properties of the speckle patterns in the new basis (the eigenvalues of the new correlation matrix). Therefore, the intensity moments—and in particular the normalized second moment—are dependent on the polarization basis.

Please note that this effect is entirely due to a statistical mechanism involving the correlation properties of single-look speckle patterns and the transformation of random variables in the polarimetric synthesis operation. It is not linked to any spatial variation of the underlying radar cross section.

The cross-polarized normalized second moment (m2xpol texture signatures) can be computed as a function of the correlation between the single-look data and their covariance matrix by numerical solution of (34), (35), and (32). We present here a few examples to illustrate this mechanism.

As a first test case, we build two-look data averaging synthesized intensities from correlated complex Gaussian speckle patterns; the measured ensemble covariance matrices are taken from the experimental data reported in [2].

A number of situations can be analyzed as a function of the correlation properties of the speckle patterns in the (H, V) basis. In Fig. 1(a) we show a family of curves for a cut in the plane corresponding to linear polarization of the m2xpol signature when $E\left[{}_1S_{\rm HH} \cdot {}_2S^*_{\rm HH}\right] = 0.5$, $E\left[{}_1S_{\rm VV} \cdot {}_2S^*_{\rm VV}\right] = 0.5$, and $E\left[{}_1S_{\rm HV} \cdot {}_2S^*_{\rm HV}\right]$ varies from 0.0 to 0.09. The two characteristic maxima at orientation angle 45° and 135° are present; this distinctive feature is also observed in experimental SAR data (see Section IX). The depth of the peak modulation is a function of the cross-polarized channel correlation: for low speckle pattern correlation the moment tends to the nominal value of

1.5 as the basis tends toward the (H, V) basis. For higher values of the correlation, the normalized moment variation with linear polarization is smoothed out, and the moment has higher values than the nominal ones even in the (H, V) basis (family of curves from red to green).

The sensitivity of the cross-polarized texture signature to the co-polarized speckle patterns correlation is demonstrated in Fig. 1(b) where the family of curves now refers to $E\left[{}_1S_{\mathrm{HH}} \cdot {}_2S^*_{\mathrm{HH}}\right]$ $E\left[{}_1S_{\mathrm{VV}} \cdot {}_2S^*_{\mathrm{VV}}\right]$ varying from 0.0 to 0.9. As the correlation between the co-polarized speckle patterns decreases (green to red color in the graphic) the cross-polarized texture signature tends to flatten out; to the limit of low correlation values the signature maxima are shifted at orientation angles 0° and 90°.

For the experimental part of this study (Section IX) JPL AIRSAR four-look data are used. In these datasets, the Stokes scattering operator is indeed derived from correlated single-look data. The absolute values of the correlation coefficients among neighboring pixels and for all polarimetric channels are of the order of 0.5 as reported in [1]. The correlation, however, dies out quickly in space, and already the correlation coefficient at the second neighboring pixel is 0.05. In order to interpret the experimental data, our model must, therefore, be modified to include four speckle patterns.

The pdf for four correlated speckle patterns is given [22] by

$$p(I) = \sum_{k=1}^{4} \frac{\lambda_k^2}{\prod_{p=1, p\neq k}^{4} (\lambda_k - \lambda_p)} e^{(-I/\lambda_k)}. \tag{36}$$

Assuming $\sum \langle I_i \rangle = 1$ and correlation coefficients $r_{12} = 0.5$ $r_{13} = 0.06$ $r_{14} = 0.06$ $r_{23} = 0.5$ $r_{24} = 0.06$ $r_{34} = 0.5$ where

$$r_{ij} = \left|E\left[S_i S_j^*\right]\right| / \sqrt{E\left[\left|S_i\right|^2\right] E\left[\left|S_j\right|^2\right]}$$

the eigenvalues of the correlation matrix are $\lambda_1 = 0.614$ $\lambda_{21} = 0.26$ $\lambda_3 = 0.124$ $\lambda_4 = 0.001$. The second-order normalized moment and the normalized standard deviation are $\overline{m}_2 = 1.459\,(\mathrm{sd/m}) = 0.678$. These values should be compared with the nominal ones for uncorrelated four-looks, which are $\overline{m}_2 = 1.25\,(\mathrm{sd/m}) = 0.5$.

Under the assumption of correlated speckle patterns in the multilook generation, speckle statistics will be accountable for a texture signature modulation in the order of magnitude indicated above.

If the single looks are correlated RVs, then the multilook average of intensities (sample mean) is no longer an unbiased minimum variance estimator (MVU) of the mean intensity. The MVU can be found casting the problem into one of variance estimator by a quadratic filter of a sequence of complex Gaussian distributed RVs. This estimator then requires complex data and is given for N looks [23] by

$$\hat{\sigma} = \frac{1}{N}\mathrm{Tr}\left(\mathbf{R^{-1}} \mathbf{s}\mathbf{s}^+\right) = \frac{1}{N}\mathbf{s}^+\mathbf{R^{-1}}\mathbf{s} \tag{37}$$

where $\mathbf{s}$ is a N-dimensional vector of random variables holding the single-look complex data. $\mathbf{R}$ is a matrix of correlation coefficients for the N single looks defined in (38) (shown at the bottom of the page).

If complex single-look data are available, one could apply the unitary transformation (6) to each single-look polarimetric vector and then estimate the mean intensity at polarization state ρ using the MVU estimator (37). In this case, polarization synthesis would have to be applied before multilooking, which limits the practicality of this approach. However, from the theoretical point of view, it is interesting to investigate what would be the impact of a polarization state change on the normalized second moment of intensity when the MVU estimator is used for multilooking, and in case of correlated speckle patterns.

$Q = \mathbf{s}^+\mathbf{R^{-1}}\mathbf{s}$ is a hermitian form. The expected value and variance of Q are given by [24]

$$E\left[\mathbf{s}^+\mathbf{R^{-1}}\mathbf{s}\right] = \mathrm{Tr}\left(\mathbf{R^{-1}C}\right) \tag{39}$$

$$\mathrm{VAR}\left[\mathbf{s}^+\mathbf{R^{-1}}\mathbf{s}\right] = \mathrm{Tr}\left(\left(\mathbf{R^{-1}C}\right)^2\right) \tag{40}$$

where $\mathbf{C}$ is the covariance matrix of $\mathbf{s}$, and Tr is the trace of the matrix.

Let us consider for simplicity the case of two correlated looks. We have

$$\begin{aligned}\frac{\mathrm{VAR}\left[\sigma\right]}{E\left[\sigma\right]^2} &= \frac{\mathrm{Tr}\left[\left(\frac{1}{2}\mathbf{R^{-1}C}\right)^2\right]}{\left(\mathrm{Tr}\left[\frac{1}{2}\mathbf{R^{-1}C}\right]\right)^2} \\ &= \left(2C_{11}C_{22}C_{12}^2C_{21}^2 + C_{11}^2C_{22}^2\left(C_{11}^2 + C_{22}^2\right)\right. \\ &\quad -4C_{11}C_{22}C_{12}C_{21}\left(C_{22}\sqrt{C_{11}C_{22}}\right. \\ &\quad \left.\left. + C_{11}\left(-C_{22} + \sqrt{C_{11}C_{22}}\right)\right)\right) \\ &\quad \cdot \frac{1}{\left(C_{11}^2C_{22} + C_{11}C_{22}^2 - 2C_{12}C_{21}\sqrt{C_{11}C_{22}}\right)^2}.\end{aligned} \tag{41}$$

Setting $E[s_1 s_1^*] = E[s_2 s_2^*]$ since the mean values of the intensities of the two speckle patterns are equal, this expression simplifies to

$$\frac{\mathrm{VAR}\left[\sigma\right]}{E\left[\sigma\right]^2} = \frac{1}{2}. \tag{42}$$

In this case, assuming perfect knowledge of the correlation matrix $\mathbf{R}$, the normalized variance would be independent of the speckle patterns' correlation matrix, and therefore, a change of polarization state would not affect it.

$$\mathbf{R} = \begin{bmatrix} 1 & \frac{|E[s_1 s_2^*]|}{\sqrt{E\left[|s_1|^2\right]E\left[|s_2|^2\right]}} & \cdots & \frac{|E[s_1 s_N^*]|}{\sqrt{E\left[|s_1|^2\right]E\left[|s_N|^2\right]}} \\ \cdots & \cdots & \cdots & \cdots \\ \cdots & \cdots & \cdots & \cdots \\ \frac{|E[s_N s_1^*]|}{\sqrt{E\left[|s_N|^2\right]E\left[|s_1|^2\right]}} & \frac{|E[s_N s_2^*]|}{\sqrt{E\left[|s_N|^2\right]E\left[|s_2|^2\right]}} & \cdots & 1 \end{bmatrix}. \tag{38}$$

All analytical results reported in this section have been validated by numerical simulations.

VIII. Polarimetric Mixture Model

The dependency of the polarimetric texture signature on the polarization state in the case of fully developed and correlated speckle patterns was derived in the previous section as a transformation of RVs. This phenomenon is due entirely to the statistical properties of the radar coherent imaging process and the way the observed data are combined to construct the intensity image; reasoning in terms of a multiplicative model, it pertains therefore to the fading variable. We now want to investigate the effect of the underlying radar reflectivity modulation; as we have seen in Section II we can postulate a multiplicative noise model where the texture variable is dependent on the polarization state and therefore gives rise to polarimetric texture. Such a model could be conceived as an extension of the multichannel model presented in [31]. This model is a generalization to the polarimetric—and more in general to the multichannel case—of the scalar statistical model of radar backscatter based on random walk in two dimensions [22]. It assumes that all channels see the same elementary scatterers in a resolution cell, or equivalently the number of steps in the random walk is the same in each channel. It is, therefore, suitable to describe the situation where a product model with a scalar texture variable holds. This situation is physically realized, e.g., for scattering from a uniform cloud of particles that obeys a first-order Born approximation. Such a case is discussed in [32]. If the layer is not seen as uniform at different polarizations (e.g., due o multiple scattering and different penetration depth), then the validity of the model would no longer hold. It would require an extension of the multichannel model in [31], where the random walk is governed by different parameters in each channel.

Instead of tackling the problem through an extension of the multiplicative model, we assume here that the polarimetric diversity in the underlying radar cross section is due to a combination or mixture of different physical scattering mechanisms. Each scattering mechanism is assumed to be polarimetrically homogeneous.

From the statistical point of view, this means that we consider in our ensemble averages resolution elements where the dominating scattering mechanisms are polarimetrically different (e.g., characterized by a different covariance matrix), although within each resolution element the assumptions for a fully developed speckle regime still holds. From the physical point of view, this situation arises, for instance, when imaging a fragmented target at the scale of the sensor's resolution.

In contrast to the extension of the scalar multiplicative model, the method proposed here does not assume any a priori polarimetric characterization of the texture variable. Therefore, it lends itself nicely to simulation approaches that make use of an empirical set of rules according to the scattering scenario; it is also quite useful to gain physical insight into the polarimetric texture observed in experimental data.

For the two-class mixture model, we assume that the polarimetric feature vector $\mathbf{x}$ has a pdf given by

$$f(\mathbf{x}, \mathbf{C_i}, \varepsilon) = (1-\varepsilon)\,\Phi_1(\mathbf{x}, \mathbf{C_{E1}}) + \varepsilon \Phi_2(\mathbf{x}, \mathbf{C_{E2}}) \quad (43)$$

which means that the feature vector is obtained from population 1 (ensemble covariance matrix $\mathbf{C_{E1}}$) with probability $1-\varepsilon$ and from a population 2 (covariance matrix $\mathbf{C_{E2}}$) with probability ε.

In case the two populations are complex Gaussian, the mixture parameters can, in principle, be estimated from experimental data using the method of moments [35]. We will deal here only with Gaussian mixtures but the model can accommodate any kind of statistical distribution.

We present next two test cases where the mixture model is used in numerical simulations. The first case deals with a mixture of a grass clutter and deterministic point targets; the second with a mixture of two vegetation classes, with different structural characteristics.

A. Clutter and Weak Point Targets

In this first scenario, we want to mimic the situation where a few dihedral reflectors are sprinkled on a vegetation background. Since the dihedral reflectors have a different polarimetric response with respect to the grass clutter, and in particular, they have no response in the cross-polarized channel and equal return and a phase shift of π in the co-polarized channel, they are supposed to introduce an imbalance in the co-polarized channels' statistics.

We suppose further that scattering from the extended target is in a fully developed speckle regime with polarimetric vectors obeying a complex Gaussian distribution. The grass clutter is modeled as a reciprocal azimuthally symmetric medium with the following covariance matrix parameters: $\sigma = 1.0\ e = 0.1\ \gamma = 1.27\ \rho = (0.61 + j0.04)$, where $\sigma = E\left[|\mathrm{hh}|^2\right]\ e = E\left[|\mathrm{hv}|^2\right]/E\left[|\mathrm{hh}|^2\right]\ \gamma = E\left[|\mathrm{vv}|^2\right]/E\left[|\mathrm{hh}|^2\right]$ and $\rho = E\left[\mathrm{hh}\cdot\mathrm{vv}^*\right]/\sqrt{E\left[|\mathrm{hh}|^2\right]E\left[|\mathrm{vv}|^2\right]}$. The dihedral is modeled by the scattering vector ($S_{\mathrm{HH}} = 1,\ S_{\mathrm{HV}} = 0,\ S_{\mathrm{VV}} = -1$). The two variables are then combined in a mixture, with the probability of occurrence for the dihedral class of 0.02. The m2xpol texture signature is computed from RVs generated by a random number generator for normal multivariate variables. The signatures of the grass clutter only and the grass clutter with the dihedrals are shown in Fig. 2.

It is interesting to notice that the polarization response does not discriminate the situation of clutter only (a) and clutter plus dihedrals (b); this is due to the fact that the mean power return of the clutter is not affected by the addition of a few weak scatterers. On the other hand the texture signature shows the two typical peaks at $\psi = (45^\circ, 135^\circ)$ in the case of clutter and dihedrals.

The polarimetric texture signature is, therefore, a powerful discriminator to detect polarimetrically diverse but radiometrically weak target embedded in a clutter, a fact that can be of importance in a number of remote sensing applications.

B. Fragmented Forest

In the second case, we consider polarimetric scattering from a natural target, a forest, and we investigate the impact of forest fragmentation on the polarimetric texture signature. Forest fragmentation refers to the situation where within the

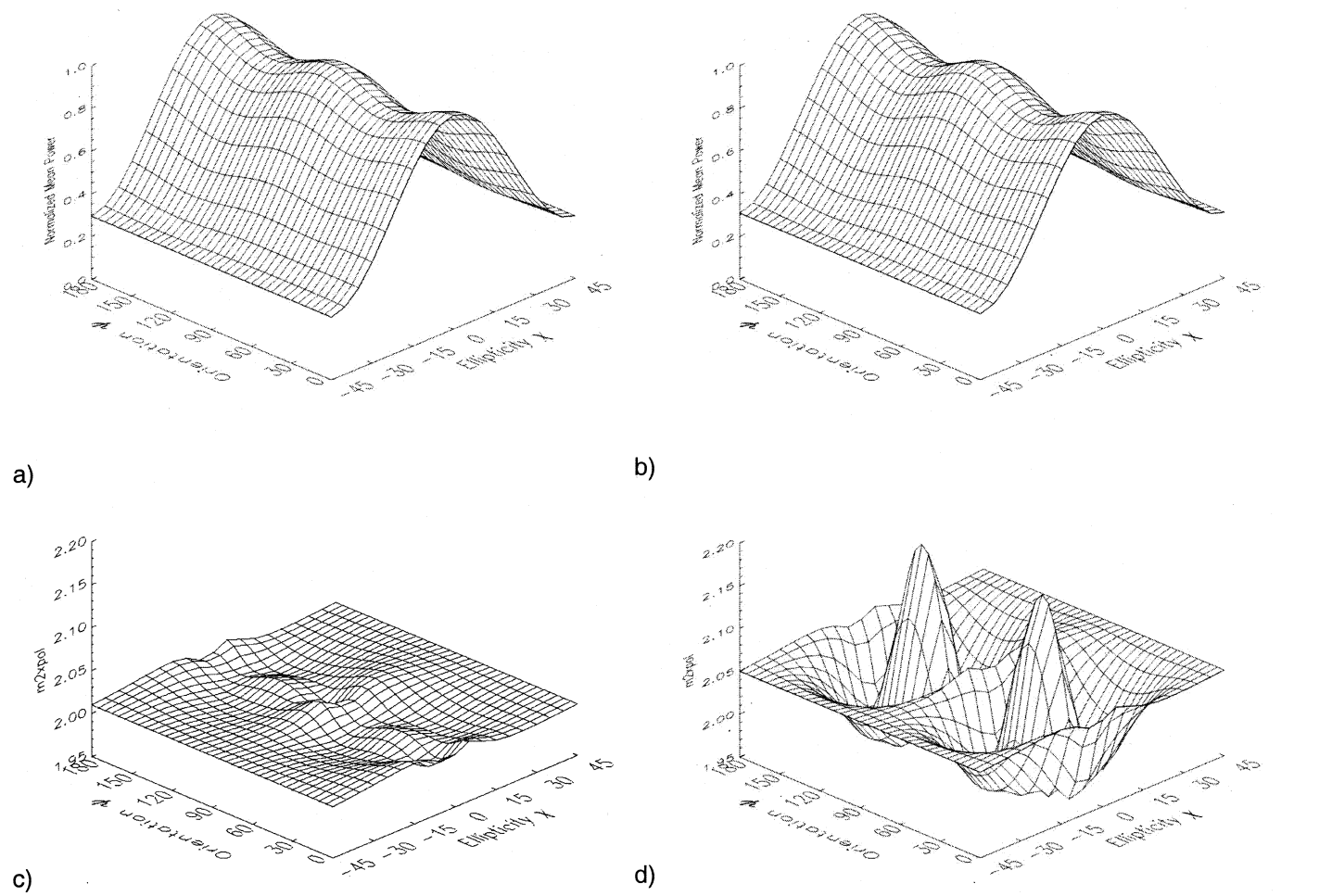

Fig. 2. Numerical simulation using the mixture model in the case of the superposition of a grass clutter and weak dihedral point targets. The co-polarized polarimetric response does not discriminate between the situation of (a) clutter only and (b) clutter plus dihedral. This is due to the fact that the mean power return of the clutter is not affected by the addition of a few weak scatterers. On the other hand, the texture signature detects remarkably well the weak dihedral targets—see frame (d) with respect to (c). Notice the two typical peaks at $\psi = (45°, 135°)$ in signature (d).

TABLE I
WAVE SCATTERING MODELING RESULTS FOR THE SIMULATION OF A FRAGMENTED FOREST

	Bush VV	**Bush HH**	**Forest VV**	**Forest HH**
Direct (canopy)	-25 dB	-30 dB	-20 dB	-40 dB
Indirect (branch-ground)	-27 dB	-25 dB	-15.9 dB	-8.2 dB
surface	-15 dB	-17 dB	-22 dB	-22 dB
total	-14.3 dB	-16.2 dB	-13.7 dB	-8 dB

field where the ensemble statistics is gathered the forest canopy and woody structure is a discontinuous function in space at the sampling interval considered. Discontinuity can arise in various situations and in different degrees; simplifying complexity in nature, we can define two cases: one where the spatial modulation is given by the addition of woody matter, the second by subtraction of woody matter. An example of the first case is the dense primary rain forest, which is composed of aggregates of many species; a profile of the upper canopy shows clusters of formations at different heights, according to the dominant specie at a point in space. An instance of the second case is the secondary forest (regrowth), where the canopy has openings at the wavelength considered (lower density) and the illuminating field penetrates down to the bushy understory and to the ground.

We take here in consideration the latter case, and we try to infer through wave scattering modeling what kind of polarimetric diversity we can expect in such a fragmented forest. The polarimetric mixture model is built in the following way.

The fragmented forest is conceptually divided into two classes with different physical parameters; the two classes, that will be referred to as *forest* and *bush*, mimic a dense broadleaf forest, and a dense understory. The physical parameters were taken from ground data used in a study for tropical ecosystem

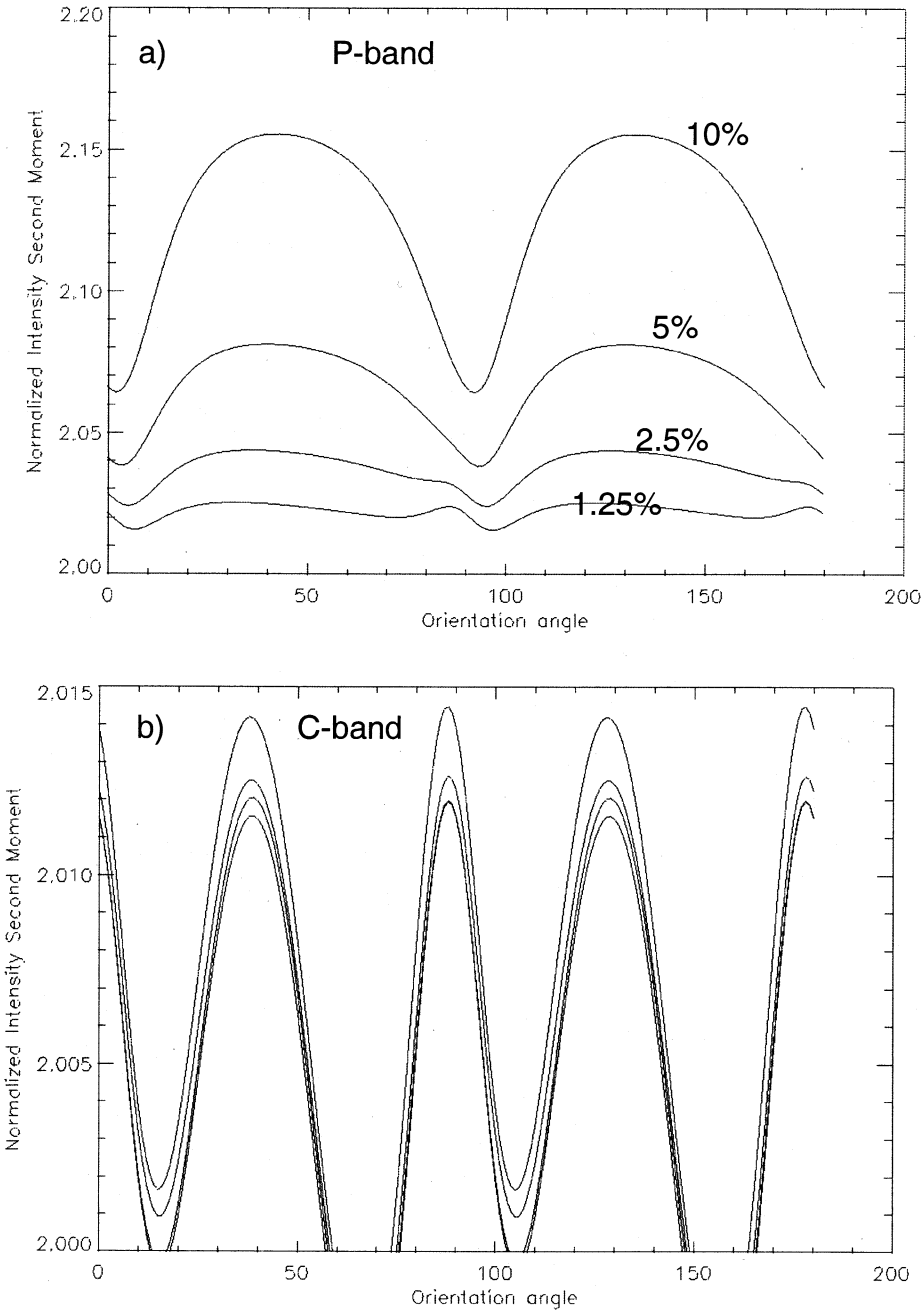

Fig. 3. Fragmented forest mixture model: m2xpol signatures (cross cut at linear polarization). (a) A family of signatures for P-band simulated data are shown parameterized by the mixture parameter. The initial mixture parameter is 10%, and it is halved for each following case down to 1.25%. As the mixture introduces more polarimetric diversity, the signature maxima at $\psi = (45°, 135°)$ become more pronounced. (b) The signature form C-band simulated data is shown, revealing a low dynamic range and a shape that is typical of the fading variable influence only.

modeling reported in [36]. A detailed description of the model parameters configuration is outside the scope of the present paper; in general terms, the forest class is modeled using three layers; the first layer from the ground is 10 m high and contains mainly the trunks, with average radius of 20 cm. The second layer is 6 m high and contains the main branches (6-cm radius and 6 m length). The upper layer contains the canopy with small twigs (ranging from 0.5–1.5-cm radius and from 60–70-cm length) and leaves (5-cm-diameter discs and 415/m^3 density). The bush class is modeled using one layer only, which is 3 m high and contains the same density and type of leaves plus four categories of branches, ranging from 0.5–2-cm radius and 0.2–1 m in length.

A layered vegetation wave scattering model [37], [38] is used to generate from the forest physical parameters the polarimetric ensemble covariance matrix. Polarimetric vectors are generated assuming a two-class complex Gaussian mixture model. Results for P-band and 25° incidence angle are summarized in Table I.

The rationale behind the chosen forest structure model is that we would expect to generate an appreciable polarimetric difference between the two classes at low microwave frequency. At P-band the incident field sees through the forest canopy the

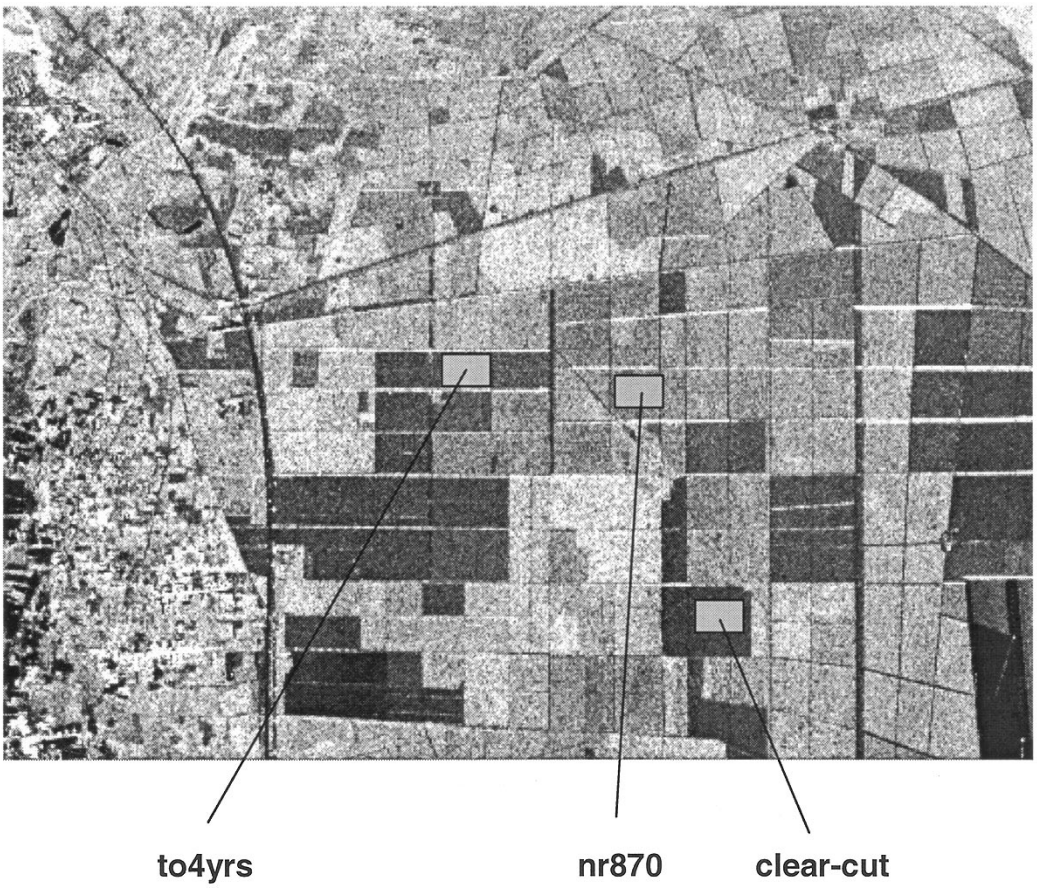

Fig. 4. JPL AIRSAR P-band image of the Les Landes forest in France acquired during the ESA/JRC MAESTRO1 1989 campaign. The image is synthesized at HH polarization. The stands highlighted by a box were used to estimate sample polarimetric texture signatures. The stands are categorized by tree ages according to the following nomenclature: *to4years*—young seedlings less than four years old; *nr870*—five to eight years old; *clear-cut*—grass land or bare soil.

underlying trunk and branch layers. Different scattering components, such as the indirect branch-ground and trunk-ground scattering, start to weigh into the total backscattered power density. Indeed at VV polarization both direct scattering from the canopy and indirect scattering (branch–soil) contribute to the total backscattered power. At HH polarization on the other hand only the indirect scattering plays a role. This creates polarimetric diversity, because the indirect scattering contribution is shared differently between the horizontal and vertical field components. For the class *bush* the effect is less relevant due to the different size and orientation distribution of the branches. Therefore, at P-band we would expect to generate a mixture of two classes with different ensemble polarimetric properties, because the indirect scattering and the direct scattering would be respectively the dominant mechanisms. At C-band on the other hand the two classes would be much more homogeneous, because the direct scattering components would be dominant in both cases, due to the lower canopy penetration.

A family of m2xpol signatures (cross cuts at linear polarization) parameterized by various values of the $\mathbf{C}_E^{\mathrm{BUSH}}$ fraction are reported in Fig. 3(a). It is first of all important to notice how even for small values of the second class fraction, the m2xpol signature switches shape toward the characteristics two peaks at (45°, 135°); moreover the range of the signature is proportional to the fraction of the class that introduces polarimetric diversity. By contrast the co-polarized and cross-polarized responses are completely invariant in shape; only the absolute values would be slightly modulated as a function of the mixture parameter. The two heterogeneous classes do not introduce polarization diversity in the first-order moment but only in the second-order moment. We can, therefore, conclude that in this case the polarimetric texture signature provides additional information about the phenomenon that we observe.

The m2xpol for the C-band simulated data is reported in Fig. 3(b). The signature does not show any appreciable variation. Therefore, at C-band no significant polarimetric texture is detected.

IX. Experimental Analysis

The polarimetric texture signature formalism introduced in Section V is an analysis tool; given an ensemble of resolution elements the signature captures in a synthetic graphical form some statistical properties as a function of the polarization basis. Like in the case of the polarimetric response, it is not directly suitable as such for classification purposes; however, polarimetric discriminators can be derived from the analysis step and used in a classification scheme (see below).

The texture signature is sensible to the following underlying mechanisms:

1) correlated speckle patterns in the multilook processing;
2) polarimetric diversity of the texture variable at first order in the polarimetric channels.

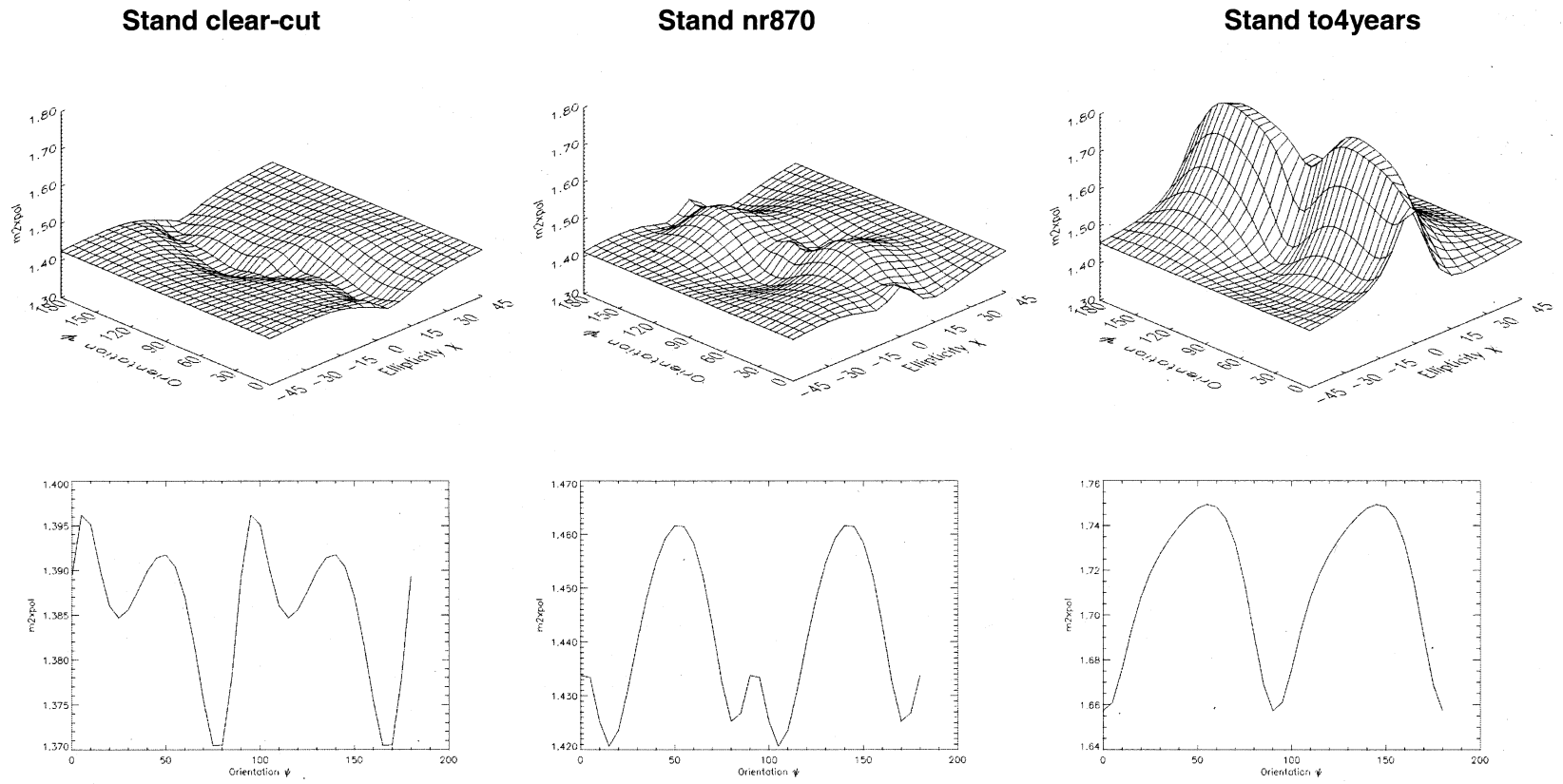

Fig. 5. Sample polarimetric texture signatures (m2xpol) estimated on the areas highlighted in Fig. 4. In the top half of the figure the 3-D signatures are shown, scaled to the absolute maximum value over all signatures. In the lower half of the figure profiles of the signatures taken at linear polarization are shown (for each graphic the y-range is set to the maximum of the signature). The difference in range of the signatures clearly indicates that two mechanisms are coming into play: the low signature fluctuation for stands *clear-cut* and *nr870* is due to speckle statistics (correlated speckle patterns); the higher dynamic range in the signature for stand *to4years* indicates the presence of polarimetric texture diversity, which can be described by a mixture model. In this case, it is due to a thin linear feature (probably a road).

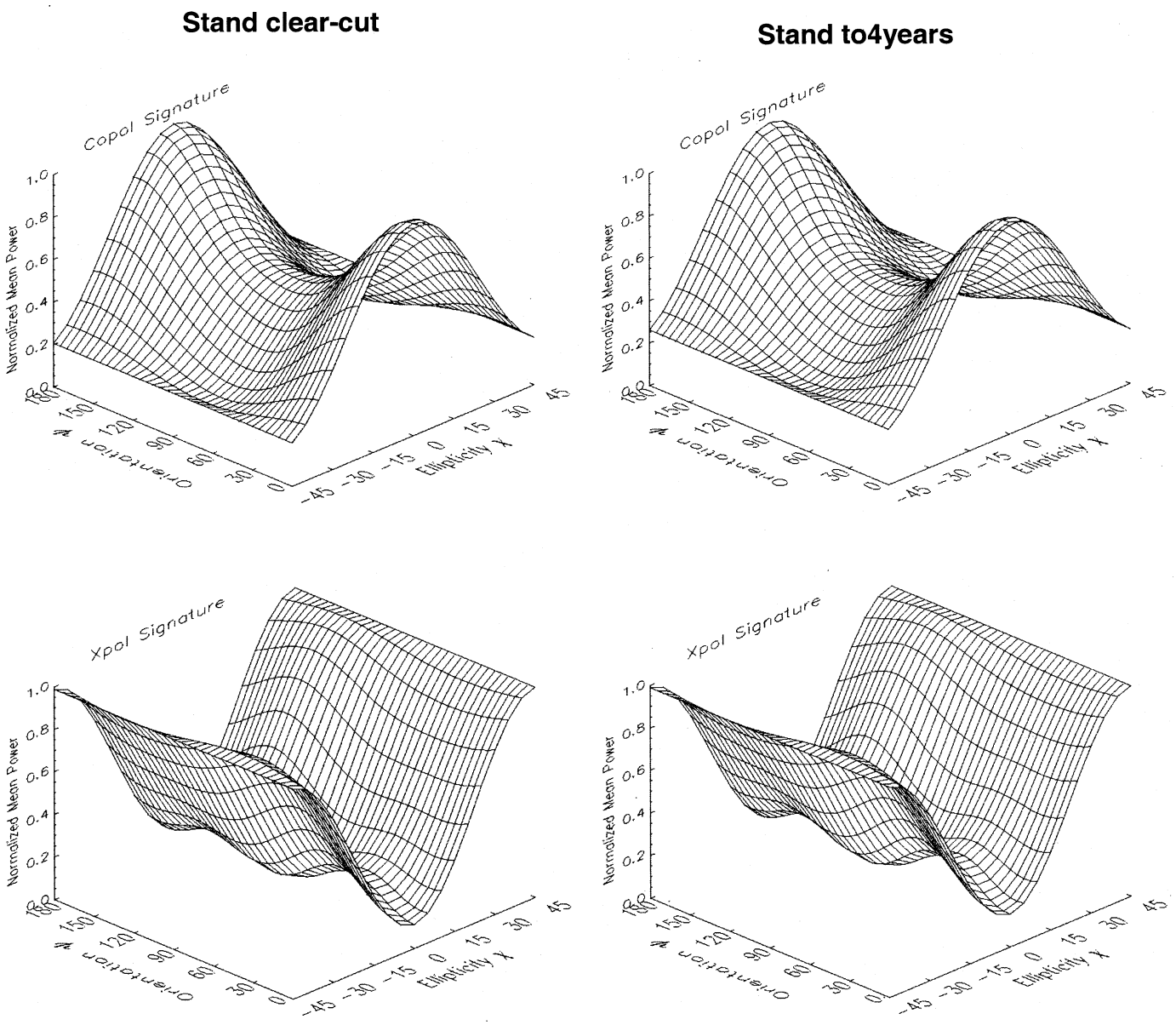

Fig. 6. Polarization response for the stands *to4years* and *clear-cut*. The two stands have similar characteristics in terms of the mean backscattered power, and therefore, the cross-polarized and co-polarized polarization responses do not show marked differences. On the other hand the polarimetric texture signatures of the two stands are quite different (see Fig. 5), which is a proof of how radiometrically similar targets can be discriminated by their polarimetric textural properties.

The last mechanism can in turn be caused by

1) partial nonstationarity in the polarimetric channels;
2) mixture of polarimetrically different scattering mechanisms.

In this section, we will discuss a number of examples of polarimetric texture signatures estimated from experimental polarimetric SAR data; the observations will be interpreted with respect to the above mentioned mechanisms, and linked to the theory and the models outlined in the previous sections.

The datasets used in this analysis were acquired by the JPL AIRSAR polarimetric radar during the 1989 MAESTRO campaign over the Les Landes forest in France. Only P-band data are discussed in this paper.

The Les Landes site is a kind of natural laboratory, where due to forest management practices, quite regular (in terms of structure and phenology) and well-documented forest stands are present. The forest stands are composed mainly of maritime pine species (Pinus Pinaster); the forest biophysical parameters are homogeneous within a stand, and span a range of values between stands, due to the different tree ages (from seedlings to over 46 years old). Also clear-cut areas are present.

Two data takes acquired on Aug. 16, 1989 are used, which cover different areas of the test site located at $(44^\circ 34', -1^\circ 0.5')$ and $(44^\circ 43', 0^\circ 52')$; the second acquisition includes also an agricultural area.

An amplitude image synthesized at HH polarization of the first target area is shown in Fig. 4. Sample polarimetric texture signatures (m2xpol) estimated on the areas highlighted in Fig. 4 are reported in Fig. 5. In the top half of the figure the 3-D signatures are shown, and they are scaled to the absolute maximum

value over all signatures. In the bottom half, profiles of the signatures taken at linear polarization are shown with the full signature range in each graphic.

The difference in absolute values in the texture signatures clearly indicates that two mechanisms are coming into play: the low signature modulation for stands *clear-cut* and *nr870* is due to speckle statistics (correlated speckle patterns see Section VII); the higher dynamic range in the signature for stand *to4years* indicates the presence of polarimetric texture diversity, which can be described by a mixture model (see Section VIII). In this case, it is due to a thin linear feature (probably a road), which is detected only at selected polarization states. The effect is, therefore, analogous to the one dealt with in Section VIII for weak point targets in a clutter. Incidentally experimental evidence of this type of phenomenon was firstly reported in [9]. For comparison the polarization response of stands *clear-cut* and *to4years* is reported in Fig. 6. Since the targets are similar in terms of the mean backscattered power, the effect of the weak nonstationarity cannot be captured by the first moment; this shows again how radiometrically similar targets can be discriminated by their polarimetric textural properties.

We have, therefore, here a clear example of the two basic underlying mechanisms that contribute to polarimetric texture. Discrimination between the two categories can be readily done by comparison with the theoretical normalized second moment values computed in Section VII. Values between 1.25 and 1.46 (corresponding to normalized standard deviation of intensity of 0.5 to 0.68) can be considered as thresholds for variation due to speckle statistics.

Also in the profiles at bottom in Fig. 5 two patterns are apparent as far as the signature maxima are concerned. The maxima positions in orientation angle are at $\psi = (0^\circ, 90^\circ)$ or at $\psi = (45^\circ, 135^\circ)$. These patterns should be compared with those in Fig. 1. The patterns are influenced in the case of the speckle statistics by the correlation coefficients between the complex speckle patterns and the ensemble covariance matrix of the target.

In the case of polarimetric texture diversity the patterns can be linked to an imbalance in the second moments of the polarimetric intensities in the (H, V) basis. This can be analyzed using the signature decomposition formalism outlined in Section VI for the linear polarization case.

For the signature with two characteristic maxima around $\psi = (45^\circ, 135^\circ)$ (e.g., stand *to4years*), inspection of the eigenshapes tells us that this shape can be generated by the functions linked to the co-polarized channels. The results of a perturbation analysis on the normalized second-order moment of the sample covariance matrix elements $E[\mathrm{hh} \cdot \mathrm{hh}^*]$ and $E[\mathrm{hh} \cdot \mathrm{vv}^*]$ vis. $A_1 = A_1 + \delta\, A_4 = A_4 + \delta$ (see Section VI) is shown in Fig. 7(a) (dashed, dotted, and solid line for increasing δ). In particular, the sensitivity is weighted by the mean intensity and, therefore, is dominated either by the HH or the VV channel imbalance.

Similar considerations can be made for the signature with two characteristic maxima at $\psi = (0^\circ, 90^\circ)$ (e.g., stand *clear-cut*). The sensitivity analysis is shown in Fig. 7(b). Here we conclude that an imbalance in the cross-polarized channel $E[\mathrm{hv} \cdot \mathrm{hv}^*]$ is the dominating factor.

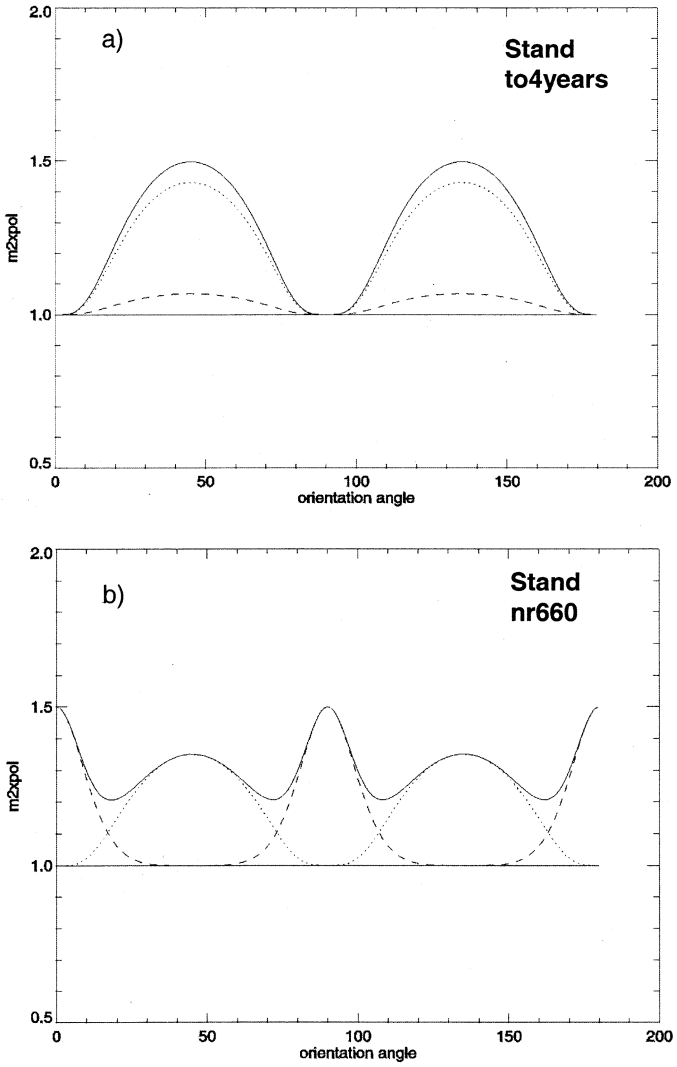

Fig. 7. Polarimetric texture signature decomposition and sensitivity analysis allow us to associate characteristic patterns of the signature maxima to the imbalance of the normalized second moments of intensity in the (H, V) basis. Analysis of the signature with maxima at $\psi = (45^\circ, 135^\circ)$ is reported in frame (a). The eigenshapes indicate in this case that the signature is sensible to an imbalance in the co-polarized channels moments (from dashed to solid line in the graph). In particular, the sensitivity is weighted by the mean intensity, and therefore, it is dominated either by the HH or the VV channel. The sensitivity analysis for a texture signature with maxima at $\psi = (0^\circ, 90^\circ)$ is reported in frame (b). In this case, the signature is sensitive to an imbalance in the cross-polarized channels moments.

One more interesting case related to nonstationarity at selected polarization states (see Section VIII) is illustrated using the data acquisition over the Les Landes site that contains agricultural areas. Here a rotating irrigation system is installed. The system is composed of a linear array of sprinklers that hinge on a central pivot. These areas exhibit extended inhomogeneities when imaged at certain polarization states due probably to differences in soil moisture. An example is shown in Fig. 8 where one of the circular irrigation areas has been selected and the amplitude image synthesized in the linear cross-polarized configuration and increasing orientation angles $0^\circ \leq \psi \leq 35^\circ$ in steps of 5°. The rectangular structure in one of the circular fields is clearly enhanced at $\psi = 0^\circ$ and fades away at $\psi = 35^\circ$.

The m2xpol signature estimated around the nonstationary feature (see area highlighted on picture frame at $\psi = 25^\circ$) and

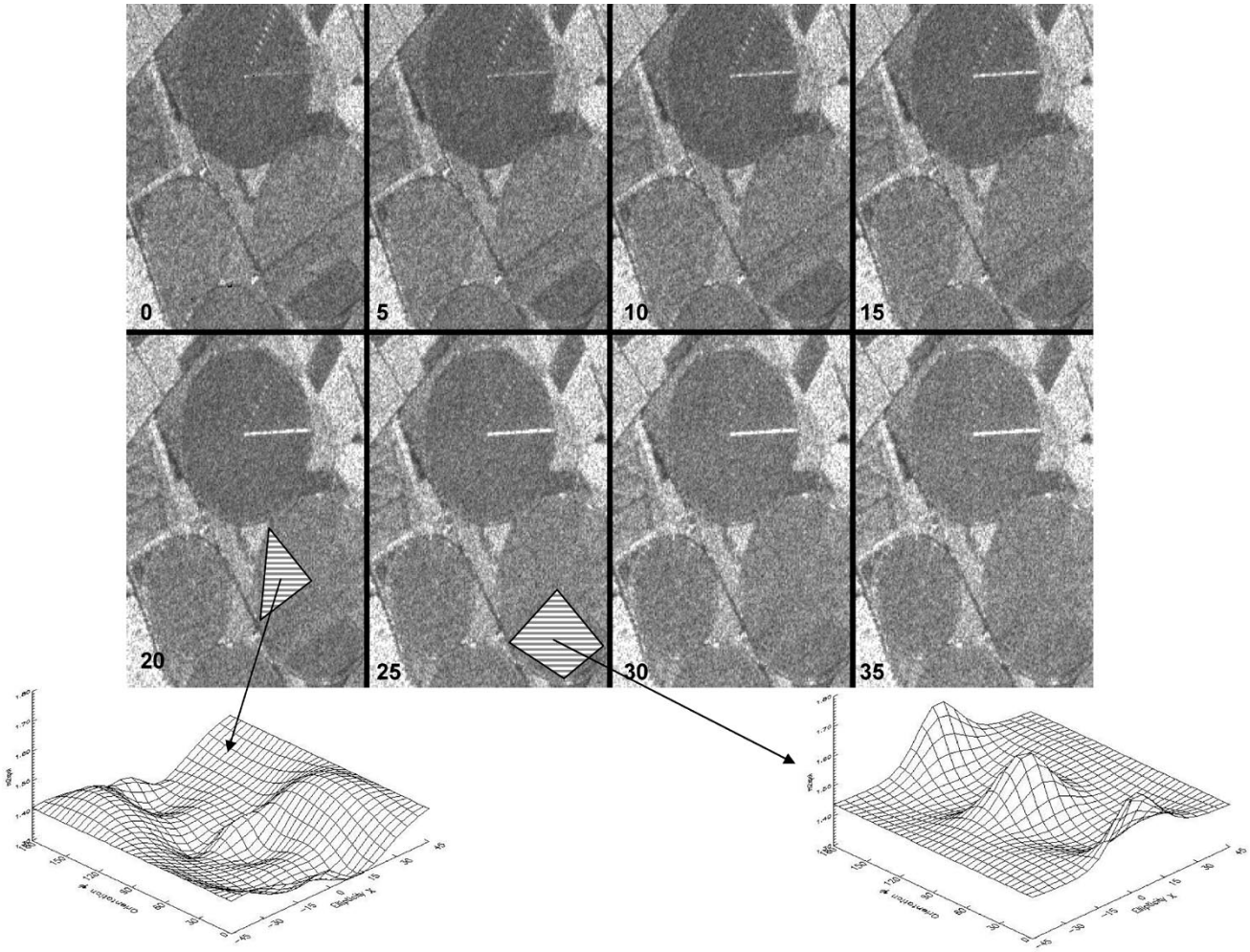

Fig. 8. Set of amplitude images of the Les Landes agricultural site. The images are synthesized in the cross-polarized linear configuration and increasing orientation angle $0^\circ \leq \psi \leq 35^\circ$ in increments of 5°. The imaged target is an agricultural area where a rotating irrigation system is installed. Different extended and point-like features become visible at different polarization states; in particular, a rectangular area is enhanced at HV polarization in one of the circular fields (highlighted by a dashed pattern). The effect is probably due to differences in soil moisture. The m2xpol signature corresponding to this nonstationary area is shown in the bottom right corner. For comparison also the m2xpol signature estimated outside the nonstationary area is shown in the bottom left corner.

the signature of a stationary area just aside (see area highlighted on picture frame at $\psi = 20^\circ$) are shown at the bottom of Fig. 8.

From the analysis steps outlined above guidelines can be inferred to implement a classification scheme based on the properties of the polarimetric texture signature. Since polarimetric texture measures require sufficient statistics to be estimated locally, we propose here a segment based labeling scheme, rather then a pixel based classifier. According to this approach only the power terms of the polarimetric covariance matrix are used at first for clustering and segmentation. In particular, we use a wavelet differential operator as a preprocessing step to arrive at an edge preserving smooth approximation of the amplitude images [39], followed by a contextual unsupervised segmentation algorithm [40]. For each segment, a local estimate of m2xpol is computed. The value of the maxima of the signature, and the difference between the maxima and the minima are used to discriminate the following situations:

1) speckle regime with constant underlying radar reflectivity and no polarimetric diversity;
2) texture with increasing degree of polarimetric diversity;
3) nondeveloped speckle (deterministic targets) or high nonstationarity due to a mixture of scattering mechanisms.

The mechanisms underpinning point 1) are described in Section VII and are related only to speckle statistics. The mechanisms in point 2) are related to the polarization diversity of the texture variable; they can be accounted for by a mixture of polarimetrically different underlying scattering processes (see Section VIII). Finally category 3) comprises targets that give local nonstationarity at selected polarization states.

As an example of the classification scheme, labeling of the segmented Les Landes forest dataset based on polarimetric texture is shown in Fig. 9. Labels correspond to the following color code: speckle regime (black); texture with increasing polarimetric diversity (from blue to orange); high nonstationarity (red).

In the same figure, also a map with a set of polygons and a legend corresponding to ground forest characterization data is shown for reference (courtesy of T. Le Toan of CESBIO). The following observations can be made.

Only some clear-cut areas and the older denser forest stands exhibit homogeneous statistical characteristics (black

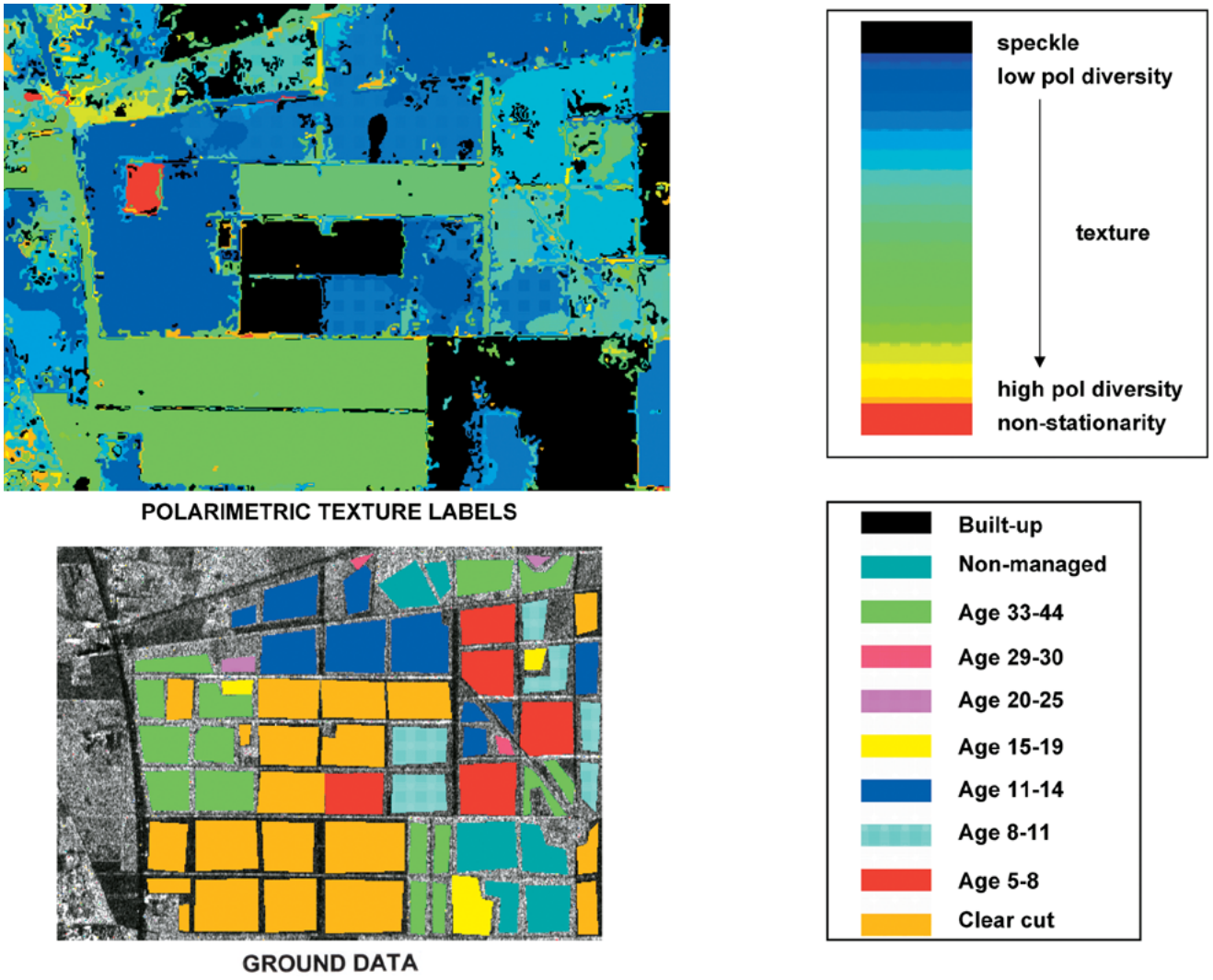

Fig. 9. Segmentation and labeling of the MAESTRO '89 Les Landes forest image based on polarimetric texture. Labels are defined according to the m2xpol signature properties (absolute values of the maxima and variance of the signature). Labeling criteria and color coding are 1) speckle regime with constant underlying radar reflectivity and no polarimetric diversity (black), 2) texture with increasing degree of polarimetric diversity (from blue to orange), 3) nondeveloped speckle (deterministic targets) or high nonstationarity due to a mixture of scattering mechanisms (red). A map with a set of polygons and a legend corresponding to ground forest characterization data is also shown for reference (courtesy of T. Le Toan of CESBIO). The texture classification map bears additional information related to polarimetric diversity with respect to a single-channel texture image.

segments). Most of the forest stands are characterized by texture but with a low degree of polarimetric diversity (blue segments). Some of the clear-cut segments show a high degree of polarimetric diversity (green areas). This is due to the fact that in the same segment different scattering mechanisms are mixed (e.g., stemming from roads and other discontinuities that are not discriminated by the segmentation algorithm). In particular, one clear-cut area (red) is labeled as highly nonstationary. Detailed examination of the HH power image showed that this is due to a weak point target embedded in the clutter. It is, therefore, a realization of the case hypothesized in Section VIII.

This segmentation and labeling exercise highlights the fact that the polarimetric texture measure proposed here adds a new dimension because it is sensitive not only to spatial discontinuities but to underlying scattering mechanisms which have a different behavior according to the polarization state.

X. Summary and Conclusion

The study presented in this paper focuses on an extension of the statistical characterization (at first order) of synthesized polarimetric SAR data when assumptions on the homogeneity of the elementary scatterers population seen from waves in different polarization states are relaxed. This situation—that we indicate as *polarimetric diversity*—can be modeled from a statistical point of view in terms of a vector texture variable in a multiplicative noise model.

We have shown from the theoretical vantage point, how, relaxing those hypotheses, new interesting effects come into play. In particular, the dependency of the normalized second-order moment of intensity on polarization state has been investigated. This dependency can be measured and condensed in graphical form by a formalism called the polarimetric texture signature. The effects predicted by the theory were confirmed by experimental analysis performed using this formalism.

It is our hope that the work presented here could have an interesting fall out both from the theoretical and practical point of view. For instance, knowledge of the statistical properties of the signal represented in a certain polarization basis can be important in problems related to optimum polarization states, such as polarimetric classifiers and speckle filters.

Practical applications could be related to the capability of discriminating weak but polarimetrically diverse scatterers from a clutter, or targets characterized by a mixture of scattering mechanisms.

Future research should focus on the validation of a multichannel classifier where polarimetric texture diversity is included, and the extension to two-point statistics characterization of synthesized polarimetric SAR data.

ACKNOWLEDGMENT

The authors would like to thank W. Boerner (University of Illinois at Chicago) for his encouragement to pursue this line of research in radar polarimetry; J. P. Malingreau, former JRC SAI MTV Head of Unit, for his moral and practical support to this work; M. Leysen, formerly a Ph.D. student at JRC, for his help in setting up the fragmented forest simulations; A. Fung and F. Amar (University of Texas at Arlington) for providing the UTA wave scattering model; G. Lemoine (JRC) for the signature decomposition method; H. De Groof and C. Lavalle (EC Joint Research Center), T. Ainsworth (Naval Research Laboratory), and F. Mattia (CNR, Italian National Research Center) for the many helpful discussions on polarimetry. Finally, the authors would like to thank the anonymous reviewers for the positive appraisal of the paper, and acknowledge that the many constructive remarks contributed significantly to improve the paper, and even stimulated new investigations.

REFERENCES

[1] J. Lee, K. W. Hoppel, S. A. Mango, and A. R. Miller, "Intensity and phase statistics of multilook polarimetric and interferometric SAR imagery," *IEEE Trans. Geosci. Remote Sensing*, vol. 32, pp. 1017–1028, Sept. 1994.

[2] J. A. Kong, A. A. Swartz, and H. A. Yueh, "Identification of terrain cover using the optimum polarimetric classifier," *J. Electromagn. Wave Appl.*, vol. 2, no. 2, pp. 171–194, 1987.

[3] I. R. Joughin, D. P. Winebrenner, and D. B. Percival, "Probability density functions for multilook polarimetric signatures," *IEEE Trans. Geosci. Remote Sensing*, vol. 32, no. , pp. 562–574, May 1994.

[4] J. J. Van Zyl, "On the importance of polarization in radar scattering problems," Ph.D. thesis, Calif. Inst. Technol., Antenna Laboratory, Pasadena, CA, 1985.

[5] J. Van Zyl, H. A. Zebker, and C. Elachi, "Imaging radar polarization signatures: Theory and observation," *Radio Sci.*, vol. 22, no. 4, pp. 529–543, July-Aug. 1987.

[6] H. A. Zebker, J. J. Van Zyl, and D. N. Held, "Imaging radar polarimetry from wave synthesis," *J. Geophys. Res.*, vol. 92, no. B1, pp. 683–701, 1987.

[7] A. P. Agrawal and W. M. Boerner, "Redevelopment of Kennaugh's target characteristic polarization state theory using the polarization transformation ratio formalism for the coherent case," *IEEE Trans. Geosci. Remote Sensing*, vol. 27, pp. 2–14, Jan. 1989.

[8] A. Q. Xi and W. Boerner, "Determination of the characteristic polarization states of the radar target scattering matrix $[S(AB)]$ for the coherent monostatic and reciprocal propagation space by using the complex polarization ratio transformation formulation," *J. Opt. Soc. Amer. A*, vol. 9, no. 3, pp. 437–455, Mar. 1992.

[9] D. R. Sheen and L. P. Johnston, "Statistical and spatial properties of forest clutter measured with polarimetric synthetic aperture radar," *IEEE Trans. Geosci. Remote Sensing*, vol. 30, pp. 578–588, May 1992.

[10] Y. Jin and S. Cloude, "Numerical eigenanalysis of the coherency matrix for a layer of random nonspherical scatterers," *IEEE Trans. Geosci. Remote Sensing*, vol. 32, pp. 1179–1185, Nov. 1994.

[11] S. R. Cloude and E. Pottier, "A review of target decomposition theorems in radar polarimetry," *IEEE Trans. Geosci. Remote Sensing*, vol. 34, pp. 498–518, Mar. 1996.

[12] J.S. Lee, G. De Grandi, M. R. Grunes, and E. Nezry, "Polarimetric signature preservation in SAR speckle filtering," *Proc. IGARSS*, vol. III, pp. 1547–1576, May 1996.

[13] J. S. Lee, M. R. Grunes, and G. De Grandi, "Polarimetric SAR speckle filtering and its implication on classification," *IEEE Trans. Geosci. Remote Sensing*, vol. 37, pp. 2363–2373, Sept. 1999.

[14] A. Lopes and F. Sery, "Optimal speckle reduction for the product model in multilook polarimetric SAR imagery and the Wishart distribution," *IEEE Trans. Geosci. Remote Sensing*, vol. 35, pp. 632–647, May 1997.

[15] A. A. Swartz, H. A. Yueh, and J. A. Kong, "Optimal polarizations for achieving maximum contrast in radar images," *J. Geophys. Res.*, vol. 93, no. B12, pp. 15 252–15 260, Dec. 1988.

[16] G. G. Lemoine and G. F. De Grandi, "Polarimetric contrast classification of agricultural fields using MAESTRO-1 AIRSAR data," *Int. J. Remote Sens.*, vol. 15, no. 14, pp. 2851–2869, 1994.

[17] J. Van Zyl, "Unsupervised classification of scattering behavior using radar polarimetry data," *IEEE Trans. Geosci. Remote Sensing*, vol. 27, pp. 36–45, Jan. 1989.

[18] F. Ulaby and J. J. van Zyl, "Wave properties and polarization, Scattering matrix representation for simple targets," in *Radar Polarimetry for Geoscience Applications*, F. Ulaby and C. Elachi, Eds. Norwood, MA: Artech House, 1990, ch. 1–2, pp. 1–52.

[19] K. Tragl, "Polarimetric radar backscattering from reciprocal random targets," *IEEE Trans. Geosci. Remote Sensing*, vol. 28, pp. 856–864, Sept. 1990.

[20] C. J. Oliver, "The interpretation and simulation of clutter textures in coherent images," *Inv. Prob.*, no. 2, pp. 481–518, 1986.

[21] G. Lemoine, "On polarimetric signatures," in *Proc. IGARSS*, vol. II, Houston, TX, 1992, pp. 913–915.

[22] J. W. Goodman, "Statistical properties of laser speckle patterns," in *Laser Speckle and Related Phenomena*, J. C. Dainty, Ed. Berlin, Germany: Springer-Verlag, 1975, ch. 2, pp. 9–74.

[23] B. Picimbono, *Random Signals and Systems*. London, U.K.: Prentice-Hall, 1993, sec. 4.8, pp. 144–146.

[24] S. M. Kay, *Fundamentals of Statistical Signal Processing—Estimation Theory*. London, U.K.: Prentice-Hall, 1993, ch. 15, pp. 512–513.

[25] J. S. Lee, K. Hoppel, and S. Mango, "Unsupervised estimation of speckle noise in radar images," *Int. J. Imaging Syst. Technol.*, vol. 4, pp. 298–305, 1992.

[26] E. Jakeman, "On the statistics of K-distributed noise," *J. Phys. A: Math. Gen.*, vol. 13, pp. 31–48, 1980.

[27] E. Jakeman and R. J. A. Tough, "Generalized K distribution: A statistical model for weak scattering," *J. Opt. Soc. Amer. A*, vol. 4, no. 9, Sept. 1987.

[28] M. C. Teich and P. Diament, "Multiply stochastic representations for K distributions and their Poisson transforms," *J. Opt. Soc. Amer. A*, vol. 6, no. 1, January 1989.

[29] S. H. Yueh, J. A. Kong, J. K. Jao, R. T. Shin, H. A. Zebker, and T. Le Toan, "K-distribution and multi-frequency polarimetric terrain radar clutter," *J. Elect. Waves Applications*, vol. 5, no. 1, pp. 1–15, 1991.

[30] F. T. Ulaby, F. Kouyate, B. Brisco, and T. H. L. Williams, "Textural information in SAR images," *IEEE Trans. Geosci. Remote Sensing*, vol. GE-24, pp. 235–245, Mar. 1986.

[31] C. Oliver and S. Quegan, *Understanding Synthetic Aperture Radar Images*. Norwood, MA: Artech House, 1998, pp. 360–364.

[32] M. L. Williams, S. Quegan, and D. Blacknell, "Intensity statistics in the distorted Born approximation: Application to C-band images of woodland," *Waves Random Media*, vol. 7, no. 4, 1997.

[33] B. Picimbono, *Random Signals and Systems*. London, U.K.: Prentice-Hall, 1993, pp. 104–123.

[34] I. R. Joughin, D. B. Percival, and D. P. Winebrenner, "Maximum likelihood estimator of K distribution parameters for SAR data," *IEEE Trans. Geosci. Remote Sensing*, vol. 31, pp. 989–999, Sept. 1993.

[35] S. M. Kay, *Fundamentals of Statistical Signal Processing—Estimation Theory*. London, U.K.: Prentice-Hall, 1993, ch. 9, pp. 289–299.

[36] G. De Grandi, M. Leysen, A. Fung, and F. Amar, "Wave scattering model of a natural target under time evolution," *Proc. IGARSS*, pp. 688–690, July 1995.

[37] A. Fung, *Microwave Scattering and Emission Models and Their Applications*. Norwood, MA: Artech House, 1994, ch. 11, pp. 451–524.
[38] M. A. Karam, A. K. Fung, R. H. Lang, and M. S. Chuahan, "A microwave scattering model for layered vegetation," *IEEE Trans. Geosci. Remote Sensing*, vol. 30, pp. 767–784, Nov. 1992.
[39] G. F. De Grandi, J. S. Lee, P. Siqueira, A. Baraldi, and M. Simard. (2001, July) Segmentation and labeling of polarimetric SAR data: Can wavelets help?. *Proc. IGARSS*
[40] A. Baraldi, P. Blonda, F. Parmiggiani, and G. Satalino, "Contextual clustering for image segmentation," *Opt. Eng.*, vol. 39, no. 4, pp. 1–17, Apr. 2000.

Gianfranco D. De Grandi (M'90–SM'96–F'02) received the doctorate degree in physics engineering (with honors) from the Politecnico di Milano, Milan, Italy, in 1973.

Since 1977, he has been with the European Commission Joint Research Center (JRC), Ispra, Italy, where he has performed research in signal processing for application areas such as gamma ray spectroscopy, data communications, and radar remote sensing. In 1985, he was a Visiting Scientist at Bell Communications Research, Morristown, NJ, where he participated in the design of METROCORE, one of the first research projects for gigabit rate metropolitan area networks. From 1997 to 2001, he was an Assistant Professor with the Faculté de Feresterie et Geomatique, Université Laval, Laval, QC, Canada. His current research interests include global-scale forest mapping using high-resolution spaceborne SAR, wavelet multiresolution techniques for the approximation and analysis of SAR imagery, topography sensing using polarimetric SAR data, and the statistics of polarimetric synthesized SAR images. He is Principal Investigator of the National Space Development Agency of Japan (NASDA), Tokyo, Japan, Global Rain Forest Mapping and Global Boreal Forest Mapping projects, the NASDA ALOS research program, and the European Space Agency ESA EO Exploitations projects.

Dr. De Grandi was elected IEEE Fellow, with the citation "For contributions to continental-scale vegetation mapping using high-resolution SAR mosaics, and in the area of information extraction from SAR data." He is a member of the IEEE Geoscience and Remote Sensing society, the IEEE Signal Processing society, and the Planetary Society, Pasadena CA.

Jong-Sen Lee (S'66–M'69–SM'91–F'97) received the B.S. degree from the National Cheng-Kung University, Tainan, Taiwan, R.O.C., in 1963, and the M.A. and Ph.D. degrees from Harvard University, Cambridge, MA.

He is Head of the Image Science Section, Remote Sensing Division, Naval Research Laboratory, Washinton, DC, where he is the Principal Investigator for several remote sensing programs on polarimetric SAR and interferometric SAR. He has developed several speckle filtering algorithms that have been implemented in many GIS, such as ERDAS, PCI, and ENVI, among others. His research covers a wide spectrum of areas, from control theory, operation research, and radiative transfer to SAR and polarimetric SAR image processing. He has investigated SAR image segmentation, inverse SAR, polarimetric SAR imagery statistics and speckle filtering, SAR polarimetry, and terrain/land-use classification and applications. He was granted a U.S. patent for the invention of a topography measurement technique using polarimetric SAR. His current research interests are in the area of SAR polarimetry, scattering signature modeling, polarimetric SAR interferometry, speckle filtering, and unsupervised classification. He has published more than 50 papers in refereed journals and more than 100 papers in conference proceedings and has given tutorials at IGARSS'97 and IGARSS'98.

Dr. Lee was presented the Best Paper Award and the Best Poster Award at the Third and Fourth European Conference on Synthetic Aperture Radar (EUSAR2000 and EUSAR2002), respectively. He has chaired and organized many sessions in international conferences and is currently an Associate Editor of the IEEE TRANSACTIONS ON GEOSCIENCE AND REMOTE SENSING.

Dale L. Schuler (M'61–SM'76–F'00) received the Ph.D. degree in electrical engineering from the Johns Hopkins University, Baltimore, MD, in 1973.

He is currently with the Remote Sensing Division, Naval Research Laboratory, Washington, DC. His research interests include electromagnetic scattering from land/ocean surfaces and geophysical parameter extraction from polarimetric SAR data. Recent research efforts have involved SAR measurement of topography, correction of SAR data for topographic effects, surface roughness, and signatures of internal waves/current fronts.

Dr. Schuler is a member of Sigma Xi, the American Geophysical Union, and the IEEE Geoscience and Remote Sensing Oceanic Engineering Societies.

Edmond Nezry was born in Toulouse, France, in 1958. He received education in aeronautical engineering and in physics. He received the DEA degree in space techniques and the Ph.D. degree in microwave (radar) remote sensing from the University of Toulouse, Toulouse, France, in 1988 and 1992, respectively.

From 1994 to 1996, he was a Senior Scientist at the Joint Research Centre, Ispra, Italy. From 1996, he was a Senior Scientist at Privateers N.V., Toulouse, France, a Dutch value-added company specializing in remote sensing applications and agrometeorology. He is currently a Senior Scientist for ParBleu Technologies Inc., Montreal, QC, Canada, a Canadian value-added company specialized in remote sensing research and applications. His main research fields concern speckle filtering, texture analysis and target detection in SAR images, SAR polarimetry, analysis of SAR time-series applied to the monitoring of agriculture, forestry and natural disasters, and complementarity between sensors. His field of interest extends also to the development of passive far detection systems and of control systems. He has published over 140 technical papers (articles, reports, communications, and monographs) on these topics and acts as a referee for peer-reviewed journals in the field. He has also published 14 papers in astronomy. He is Principal Investigator of JERS-1, TRMM (Japan), ERS-1, ERS-2, ENVISAT (Europe), and RADARSAT-1 (Canada) research and application projects.

Dr. Nezry is a member of GEOS, the Planetary Society, the Optical Society of America, and an honorary member of the Research Board of Advisers of the American Biographical Institute and of the International Biographical Centre.